Arabian Journal of Chemistry (2022) **15**, 104104

King Saud University

Arabian Journal of Chemistry

www.ksu.edu.sa
www.sciencedirect.com

ORIGINAL ARTICLE

Novel Cr(III), Ni(II), and Zn(II) complexes of thiocarbamide derivative: Synthesis, investigation, theoretical, catalytic, potentiometric, molecular docking and biological studies

Zehbah Ali Mohammed Al-Ahmed

Department of Chemistry, College of Sciences and arts, Dhahran Aljanoub, King Khalid University, Abha, Saudi Arabia

Received 19 April 2022; accepted 4 July 2022
Available online 08 July 2022

KEYWORDS

Thiocarbamide;
Triazole;
Complexes;
Structural optimization;
Biological assay

Abstract Throughout this research, the thiocarbamide derivative (H_2L), and its Cr(III), Ni(II) and Zn(II) complexes have been reported. The thiocarbamide moiety was established with a reaction of benzoyl isothiocyanate and 1*H*-1,2,4-triazol-3-amine. Structural elucidation of such compounds was achieved using elementary examination, spectral and magnetic experiments. The octahedral construction of the Cr(III) complex, the tetrahedral geometry of the Zn(III) complex and the mixed geometry (tetrahedral and square planar) of the Ni(II) complex have been verified by the optimization of structure using DFT. The action of Zn^{2+} complex in the oxidative degradation of an organic azo-dye was investigated, and it showed promising results. The thermal degradation behavior of thiocarbamide metal complexes were studied as well as the calculation of the kinetic data for title compounds (E_a, A, ΔH^*, ΔS^* and ΔG^*) of thermal degradation steps has been tested utilizing two different techniques. Liver carcinoma (HePG2) and breast carcinoma (MCF-7) cytotoxicity as well as ABTS-antioxidant activities demonstrated the effective inhibitory of the Ni(II)-complex relative to other tested compounds. The antimicrobial activity of the compounds suggests that Cr(III) has the highest activity. Furthermore, the Molecular Operating Environment (MOE) program was used to calculate the binding affinity between the EGFR protein and the compounds under investigation.

1. Introduction

Substituted thiocarbamides and their transition metal complexes are one such group of compounds that have promise anticancer activity (Pandey et al., 2019; Pandey et al., 2018). These compounds are more effective anticancer agents, most likely due to the presence of intramolecular hydrogen bonding in the structural framework, which increases lipophilicity and

E-mail address: zalshwal@kku.edu.sa
Peer review under responsibility of King Saud University.

Production and hosting by Elsevier

https://doi.org/10.1016/j.arabjc.2022.104104
1878-5352

improves hydrogen bonding interactions with DNA (Mahendiran et al., 2018). The coexistence of hard nitrogen, oxygen, and soft sulphur donor atoms in the structural motif of substituted thiocarbamides (Pandey et al., 2019; Almalki et al., 2021; Al-Qahtani et al., 2021; Alkhamis et al., 2021; Abu-Dief et al., 2021) gives rise to structural variety in transition metal complexes. Moreover, ligands contains triazole moiety and their derivatives show an essential function as an antimicrobials (Emam et al., 2020; Gaber et al., 2020), anticancer (Gaber et al., 2020) and antitumoral (Matesanz et al., 2020). The significance of thiourea chemistry was improved by association with metal ions which strengthen antimicrobial activity (Maalik et al., 2019), antioxidant activity (Maalik et al., 2019; Rahman et al., 2020) and anticancer activity (Maalik et al., 2019; Abbas et al., 2020). Also, thiourea derivatives offers excessive promise as a metal transition sensor ionophore (Yahyazadeh and Ghasemi, 2013; Fakhar et al., 2016; Razak et al., 2020). Because of dyes' resistance to aerobic digestion and their stability toward heat, light, and oxidizing agents (Robinson et al., 2002; Han and Yun, 2007), many challenges arise when attempting to handle wastewater-containing dyes. Such dyes are toxic, carcinogenic, and mutagenic (Anliker, 1979; Chung and Stevens, 1993). Catalytic oxidation has recently been reported as a viable technique for curing colored water (Santos et al., 2009). Metal complexes are important cellular components that participate in a variety of biochemical processes in living organisms. Minerals have a variety of properties, such as reactivity to organic substrates, altered coordination patterns, and redox activity, to name a few. As a result, developing special coordination complexes, whether drugs, is regarded as a primary goal in the development of effective diagnostic tools (Hambley, 2009). Several bioactive minerals are being studied for their potential use in the development of new pharmaceuticals. Transition metals such as Co(II), Cr (III) and Zn(II) are required for many biological processes such as electron transfer and catalysis, and they are commonly found in enzyme or protein active sites (Thompson and Orvig, 2003).

As a result of the extensive range of biological properties (Pandey et al., 2019; Pandey et al., 2018; Emam et al., 2020; Gaber et al., 2020; Matesanz et al., 2020) of thiocarbamides and triazole and derivatives, the preparation of the thiocarbamide derivative and its Cr(III), Ni(II) and Zn(II) chelate is recorded in the current research. According to the spectral and theoretical studies, various types of chelation have been suggested for metal complexes. Furthermore, the isolated Zn (II) complex's catalytic activity was reduced during the decomposition of organic Erichrome Black T (EBT) dye. Moreover, zeta potential estimation, molecular docking calculations, antimicrobial and antioxidant activities of the investigated compounds were evaluated.

2. Experimental

2.1. Materials

Solvents, metal(II) chlorides, benzoyl isothiocyanate and 1*H*-1,2,4-triazol-3-amine have been purchased from Sigma-Aldrich.

2.2. Instrumentation

PerkinElmer-2400 series-II analyzer have been used for partial elemental analysis. Ordinary methods (Jeffery et al., 1989) were being used to estimate the content of chloride and metal in investigated complexes. The Infra-red spectra were measured by KBr pellets via FT-IR spectrophotometer ''Mattson 5000″. The electronic spectra are analyzed by via UV / Vis Spectrophotometer (Unicam). The NMR spectra of ^{1}H and ^{13}C with Brucker 400 MHz were handled on ligand H_2L that is identified in the solvent (DMSO). The photoluminescence spectra of investigated compounds were made in DMSO solution on excitation by using a LS50B PerkinElmer Fluorimeter. Jenway 4010- conductivity meter was used to assess the molar conductivity of prepared DMSO solution of metal complexes (0.001 mol/dm^{-3}). The spectrum of X-ray diffraction was described in detail utilizing Cu, Wavelength 1.5406 Å source on diffractometer "the Bruker AXS Advance''. Mass spectra were obtained with ionization mode (EI) in the range of m/z = 40–1000 with Varian Mat 311. The Gouy procedure for scientific magnetic susceptibility to Sherwood has been used to determine the effective magnetic moment μ_{eff}, at room temperature per metal atom. The zeta potential measurements for the H_2L and its metal complexes in water were performed via Malvern Zeta-size Nano at 25 °C. The thermal analyzer TGA-50H was used for thermal evaluation (TGA / DTG) under measured conditions such as the temperature rises by rate equal to 10 °C/min.

2.3. Synthetic procedures of ligand, H_2L and its complexes

The H_2L ligand derived from thiocarbamide moiety and metal chelates have been synthesized in accordance with the procedures described in Scheme 1. The products obtained were crystallised a number of times with absolute EtOH then with Et_2O and then desiccated over anhydrous calcium chloride. TLC was performed to verify the purity of the H_2L ligand. The physical and analytical results are summarized in Table 1.

2.4. Molecular modelling

Unfortunately, we could not get single crystals from the investigated compounds, thus structure optimization data have been measured with DMOL^3 application in the Materials Studio software (Delley, 2002). Optimized complex frameworks were estimated using the DFT (Modeling and Simulation Solutions for Chemicals and Materials Research and Studio, 2011) process. Computations of DFT semi-core pseudopods (dspp) have been generated *via* double number basis sets and functional polarisation (DNP) (Warren, 1986) that was much additional successful than the duplicate gaussian basis groups (Kessi and Delley, 1998). Furthermore, The optimistic interchange-correlation feature was based on the functional (GGA) and (RPBE) (Hammer et al., 1999).

2.5. Catalytic oxidative degradation of EBT dye

The organic dye was oxidatively degraded at a pH 7.0 (buffered aqueous solution) in an air atmosphere in the presence

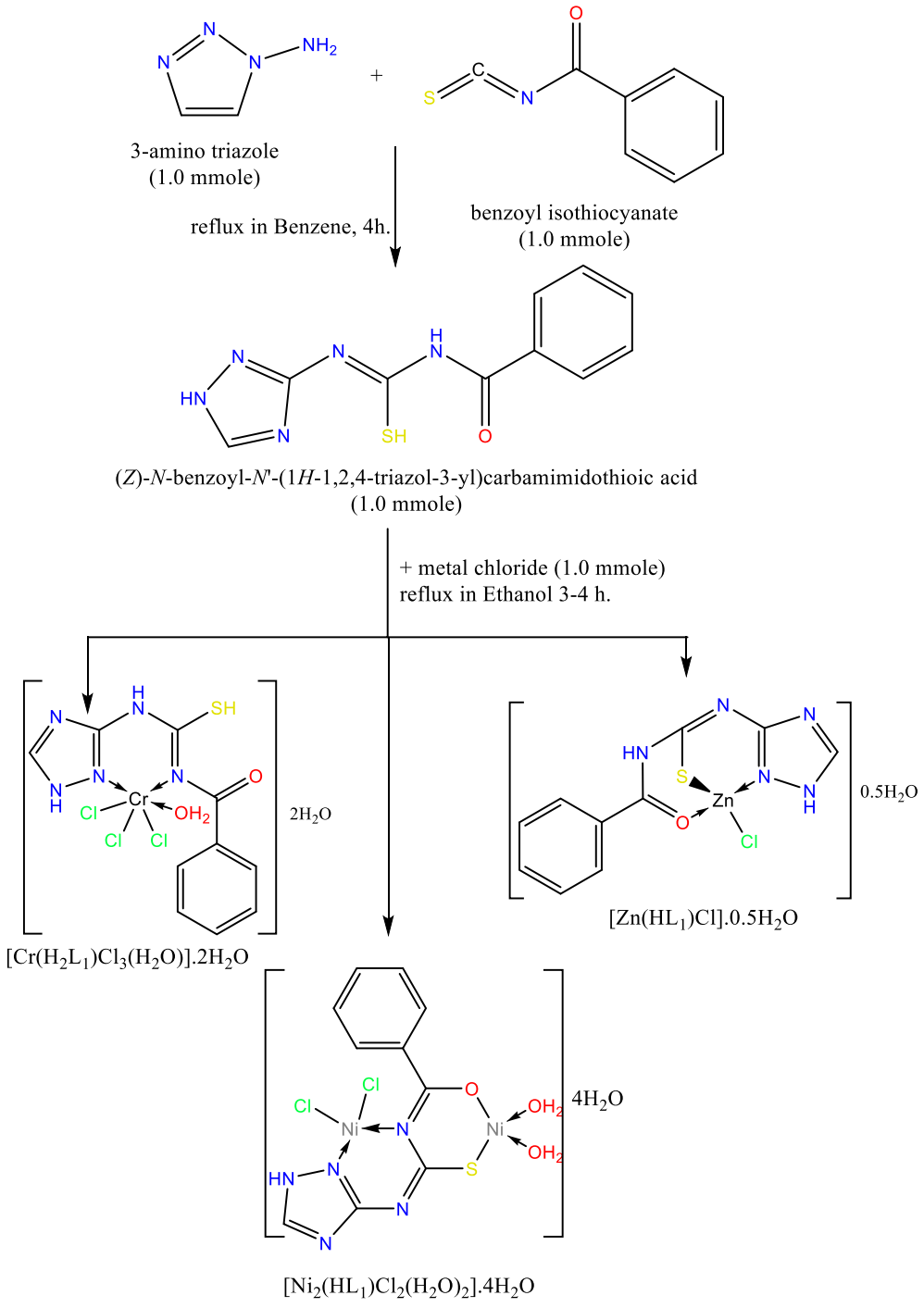

Scheme 1 The outline synthesis of ligand (H_2L) and its metal complexes.

of known doses of green oxidizing agent H_2O_2. 0.2 mg of the Zn^{2+} complex as a catalyst was added to 10 ml of the dye solution (30 mg/l), followed by an appropriate dose of H_2O_2 (30%) and stirring. At the end of each experiment, the flask contents were filtered, and the concentration of the dye in each filtrate was measured at λ_{max} of 530 nm (Hassani et al., 2015). At a constant dose of H_2O_2 (0.2 ml) and constant dye concentration (30 ppm), the effect of time was investigated by running the reaction for 5-, 10-, 15-, 20-, and 30-minute intervals. Initially, the effect of temperature was investigated by performing the reaction at 30, 45, and 60 °C. Finally, the effect of H_2O_2 dose was investigated using 0.2, 0.3, 0.4, 0.5, and 0.6 ml of H_2O_2 and constant dye concentration (30 ppm and 30 °C, respectively).

2.6. Potentiometric study

Hana Instrument 8519 digital pH meter was used to perform pH-metric measurements. Titrations were carried out at 298, 308, and 318 K. The Van Uitert and Hass relation (Uitert

Table 1 Analytical and physical data of ligand (H_2L) and its complexes.

Compound molecular formula	(F.Wt)	color	m.p. (°C)	Found (calcd.)% M	Cl	C	H	N	yield %
H_2L $C_{10}H_9N_5OS$	247.28	yellow	240	–	–	48.48 (48.57)	3.61 (3.67)	27.90 (28.32)	80
$[Cr(H_2L)Cl_3(H_2O)].2H_2O$ $C_{10}H_{15}Cl_3CrN_5O_4S$	459.68	black	245	11.42 (11.31)	22.64 (23.14)	25.64 (26.13)	3.16 (3.29)	15.54 (15.24)	90
$[Ni_2(HL)Cl_2(H_2O)_2].4H_2O$ $C_{10}H_{19}Cl_2Ni_2N_5O_7S$	541.64	dark green	290	22.15 (21.67)	13.53 (13.09)	21.92 (22.18)	3.28 (3.54)	12.85 (12.93)	93
$[Zn(HL)Cl]0.0.5H_2O$ $C_{10}H_9ClZnN_5O_{1.5}S$	356.11	white	271	18.16 (18.36)	10.20 (9.96)	33.29 (33.73)	2.69 (2.55)	19.74 (19.67)	79

and Haas, 1953) is used to correct pH-meter readings in a 50 percent (v/v) dioxane-water mixture:

$$-\log[H^+] = B + \log U_H^o + \log \gamma_{\pm}$$

Where $\log U_H^o$ and $\log \gamma_{\pm}$ are the correction factors for the solvent composition and ionic strength, respectively and B is the reading.

The titrations of solution mixtures towards standardized free carbonate NaOH solution ($9.65x10^{-3}$ M) in 50 percent (v/v) water - dioxane at constant ionic strength are used in the experiment (1 M KCl solution). Figure S1, Supplementary Materials, depicts this. The solution mixtures were made in the following manner:

a. 1.25 ml HCl (1.04×10^{-2} M) + 1.25 ml KCl (1 M) + 10 ml bidistilled H_2O + 12.5 ml dioxane.
b. 1.25 ml HCl (1.04×10^{-2} M) + 1.25 ml KCl (1 M) + 2.5 ml (5×10^{-3} M) H_2L + 10 ml bidistilled H_2O + 10 ml dioxane.
c. 1.25 ml HCl (1.04×10^{-2} M) + 1.25 ml KCl (1 M) + 2.5 ml (5×10^{-3} M) H_2L + 9.5 ml bidistilled H_2O + 10 ml dioxane + 0.5 ml metal ion (Ni^{2+}) (5×10^{-3} M).

2.7. Biological activity

2.7.1. Antimicrobial activity

The antimicrobial activity of H_2L and its respective complexes was examined against *Aspergillus flavus* fungus and *Candida albicans* fungus (ATCC 7102) as well as the bacteria G-bacteria: *Escherichia Coli* (ATCC 11775) and G+: *Staphylococcus Aureus* (ATCC 12600) by a modified disc dispersion methodology (Scheme S1, additional materials); Kirby-Bauer testing (Pfaller et al., 1988). The solution from individual substance, of investigated compounds and standard drug (Amphotericin B Antifungal Agent and Ampicillin Antibacterial Agent) in DMSO solution, were arranged for testing against spore germination. The inhibition regions diameter was expressed in millimetres (Abu-Dief et al., 2021; Aljohani et al., 2021; Abdel-Rahman et al., 2016; Abu-Dief et al., 2020).

2.7.2. Cell proliferation assay

Mammary gland (MCF-7) breast cancer, and hepatocellular carcinoma HepG2 liver cells have been established using a technique stated by Mauceri, H.J.et *al* (Mauceri et al., 1998). Percentage of relative cell viability was determined by:

$$Therelativecellviability\% = \frac{A_{570}\,\text{of Treated Samples}}{A_{570}\,\text{of Untreated Samples}} \times 100$$

2.7.3. ABTS free radical and scavenging activity

2 ml of 2,2′-azino-bis(3-ethylbenzothiazoline-6-sulfonic acid) (ABTS) solution (60 mM) and 3 ml of MnO_2 solution (25 mg / ml) was added to each of the studied compounds as well as all solutions have been prepared in 5 ml of buffer solution with pH 7, using 0.1 M of aqueous phosphate. The mixture was stirred, centrifugated, filtered, and the absorption at λ734 nm of the produced green–blue solution (ABTS radical solution) was attuned to about 0.5. The spectroscopical grade of phosphate buffer / MeOH was then applied to the 50 ml (2 mM) solution of the examined species (1:1). Absorption was measured and the decrease in colour was stated as a percentage of inhibition. L-ascorbic acid is a regular antioxidant as a positive control. while sample without ABTS was a negative control (Lissi et al., 1999; El-Gazzar et al., 2009; Aeschlach et al., 1994).

The inhibition% of free radical ABTS was calculated by the equation:

$$I\% = (Ablank - Asample)/(Ablank) \times 100$$

2.8. Molecular docking with EGFR protein

A large number of studies have shown that epidermal growth factor receptor (EGFR) is a potential therapeutic target for the treatment of various tumors (such as colorectal and breast tumors) (Avdović et al., 2020). The inactivation of this receptor can affect the spread of cell cancer and promote cancer cell apoptosis. thus, we analyzed the potential inhibitory effects of ligand, H_2L and its metal complexes.

Molecule Operating Environment (MOE) software is used to evaluate the binding affinity between EGFR protein and investigated molecules (Integrated Computer-Aided Molecular Design Platform, Molecular operating environment, Chemical Computing Group, 2019). Use the specified minimization algorithm to minimize the energy of all 3D molecule structures. Then the charge of the atom is processed and the minimized potential energy is corrected. The inspected target substances are saved as a new database in MDB format (Shah et al., 2020). The crystal structure of the EGFR receptor (PDB: 3W2S) is taken from the protein database (Sogabe et al., 2013). MOE has been used to adjust the structure of molecularly bound proteins by removing ligands,

adding hydrogen, and minimizing the energy of 3W2S. The minimized energy structure is used more as a binding receptor. The largest active center of 3W2S (PHE 856, LYS 745, ASP 855, CYS 797, ARG 841, ASN 842, MET 793, LEU 718, GLY 719, SER 720, VAL 726, ASP 800, and PHE 997) is the MOE position obtained by the site finder algorithm. The docking uses various features (initial re-scoring methodology: London dG with poses 10, final re-scoring methodology: GBVI/WSA dG with poses 5, placement: triangle matcher, and refining: rigid receptor) to identify and evaluate the compounds' connections with 3W2S. The S value is a rating value that measures the affinity of a compound to the receptor and is calculated by the standard MOE rating function. The RMSD is also used to compare the binding conformation with the binding reference configuration.

3. Results and discussion

Quantitative and spectrometric results of the ligand, H_2L and its coordinated metals suggest that the metal–ligand stoichiometry is 1:1 for all complexes except the Ni(II) complex, that has 2:1 (M: L) stoichiometric ratio. The synthetic procedure of the planned complex structure is displayed in Scheme 1. The designed complexes were stable, and insoluble in the most popular organic solvents, excepting DMSO and DMF. The molar conductivity of the synthetic compounds is of a non-electrolytic behavior.

3.1. ^1H and ^{13}C NMR spectra of H_2L

The H_2L ^1H NMR spectrum (Figure S2, Supplementary Materials) in DMSO solution showed two signals related to SH and NH protons at 11.855 and 8.445 ppm, respectively. the presence of SH signal indicated that H_2L solution was in the form of thiol. All previous signals have vanished by addition D_2O (Figure S3, Supplementary Materials). The aromatic ring protons have been found between 7.334 and 7.880 ppm.

The ^{13}C NMR spectrum (Figure S4, Supplementary Materials) revealed three signals related to the C-S and C = O carbons at 168.30 and 166.00 ppm, respectively (Hosny et al., 2021; Hosny et al., 2018). Signals occurring at 151.86, 153.62 and 158.78 ppm attributed to the C = N carbon atoms of the hetero ring and the open chain, separately.

3.2. ^1H NMR spectra of Zn(II)-complex

The ^1H NMR spectrum of Zn(II) complex (Figure S5, Supplementary Materials) in DMSO solution showed the signal related to NH proton at 8.449 ppm as well as the disappearance of signal attributed to SH proton which confirmed the proposed structure of Zn(II) complex.

3.3. IR spectra of H_2L and its complexes

A brief evaluation has been made between the Infra-Red spectral data of the H_2L ligand and its complexes in order to investigate the coordination action of H_2L towards the metal ions. The most significant IR bands of absorption were displayed in Table 2 and Figure S6, Supplementary Materials. The IR spectrum of H_2L shows distinct vibrations at 1612, 1638, 1697 and 2053 cm^{-1}, related to $\nu(C = N)_{ring}$, $\nu(C = N)^*$, $\nu(C = O)$ and $\nu(SH)$, respectively (Rakha, 2000; Abdel-Monem et al., 2018; Abdel-Monem and Abouel-Enein, 2017; Hosny et al., 2018; Abdel-Rhman et al., 2019). The intense vibration at 2053 cm^{-1}, due to the $\nu(SH)$ group, indicates that, H_2L is existing as thiol form in the solid phase. The vibrations referring to $\nu(NH)$ groups cannot be determined since a large destruction of 3160–3400 cm^{-1} overshadows their asymmetrical and symmetrical vibrations. The bending system δ of the $(C = N)_{ring}$ appeared at 623 cm^{-1}, which has changed to a larger wavenumber when it is participate in complexing.

In the Cr(III) complex, the H_2L coordinates the Cr(III) ion as neutral bidentate via the recently formed groups of $(C = N)^*$ and $(C = N)_{hetero\ ring}$. This type of complexation is indicated by the presence of $\nu(SH)$ and $\nu(C = O)$ at the higher and same wavenumbers, separately. This shows that these locations are not participate in coordination. Furthermore, the change of $\nu(C = N)^*$ to the lower wavenumber and the change of $\nu/\delta(C = N)_{triazole\ ring}$ to lower and higher wavenumbers (Rastogi and Sharma, 1974), respectively, indicated mutual coordination between these locations. In addition, in Zn(II) chloride complex, the H_2L works as mono-negative tridentate via deprotonated-SH, (C = O) and (C = N) ring groups. This statement was concluded by the absence of $\nu(SH)$ (Pandey et al., 1993), the change of $\nu(C = O)$ to less wavenumber (Abdel-Monem and Abouel-Enein, 2017) and the change of δ and ν of (C = N) ring to higher and lower wavenumbers, respectively (Abdel-Monem et al., 2018). Finally, the H_2L operates as a binegative tetradentate throughout the binuclear Ni(II) complex. This proposal is verified by the disappearance of both $\nu(C = O)$ and $\nu(SH)$ (El-Sawaf et al., 2020) with the parallel presence of $\nu(C = N)^{**}$ and $\nu(C\text{-}O)$ (Liu et al., 2012) as well as the changing of $\nu/\delta(C = N)$ vibrations (Rastogi and Sharma, 1974; Pandey et al., 1993).

Recent vibrations in regions 410–470 and 511–585 cm^{-1} were related to $\nu(M-N)$ (Ferraro and Walker, 1965) and $\nu(M-O)$, respectively. As well, the wide vibrations at $\approx$ 3432–3380 cm^{-1} confirm the existence of H_2O in the complex (Chubar et al., 2003). The values of weight loss from the

Table 2 IR bands of ligand (H_2L) and its complexes.

Compound	$\nu(C = O)$	$\nu(SH)$	$\nu/\delta(C = N)_{ring}$	$\nu(C = N)^*$	$\nu(C = N)^{**}$	$\nu(C\text{-}O)$
H_2L	1697	2053	1612, 623	1638	—	—
$[Cr(H_2L)Cl_3(H_2O)].2H_2O$	1702	2081	1576, 654	1623	—	—
$[Ni_2(HL)Cl_2(H_2O)_2].4H_2O$	—	—	1571, 649	1623	1612	1169
$[Zn(HL)Cl]0.0.5H_2O$	1671	—	1603, 630	1632	1565	—

* : azomethine. **: new azomethine.

TGA data were used to distinguish between coordinated and crystallised H_2O.

3.4. Electronic spectra, optical band gap and magnetic properties

The electronic spectra of ligand (H_2L) as well as metal complexes were recorded in DMSO solution have been revealed in (Table S1, supplementary materials and Figure S7, supplementary materials). The ligand H_2L presented bands in the ranges 242 and 216 nm, that could have been allocated to the $(\pi \rightarrow \pi^*)_{Ar}$ and $(\pi \rightarrow \pi^*)_{ring}$ transitions, respectively (Tossidis et al., 1987). The band at a value of 300 nm is due to the carbonyl moiety $n \rightarrow \pi^*$ transition (Tossidis et al., 1987). The electronic spectra of Cr(III) complex shows three absorption bands at 610, 450 and 336 nm attributable to $^4A_{2g}(F) \rightarrow {}^4T_{2g}(F)(\nu_1)$, $^4A_{2g}(F) \rightarrow {}^4T_{1g}(F)(\nu_2)$ and $^4A_{2g}(F) \rightarrow {}^4T_{1g}(P)(\nu_3)$ transitions, respectively characteristic for octahedral Cr(III) complexes (Parmar et al., 2010). Furthermore, the magnetic moment value, ($\mu_{eff.}$ = 3.36B.M.) can be taken as an extra indication for the octahedral geometry of Cr(III) complex. The complex, [Ni_2(-

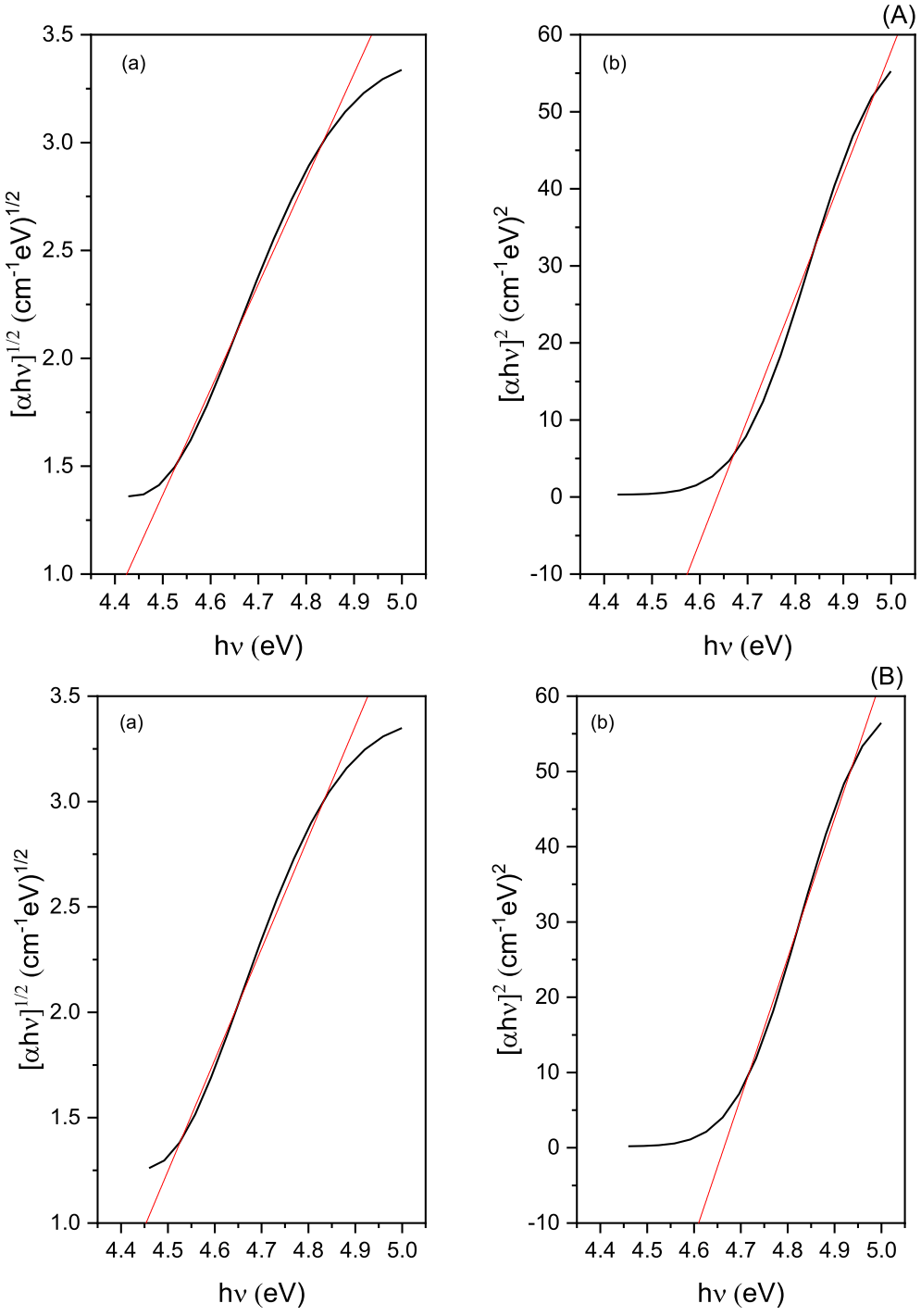

Fig. 1 Optical band gaps (a: indirect, and b: direct band gap) for A: Cr^{3+}, and B: Ni^{2+} complexes.

$HL_1)Cl_2(H_2O)_2].4H_2O$ complex have a magnetic moment values 2.63B.M., which is lesser than the measured value for a single nickel atom of d^8-octaedral and/or tetrahedral complexes and larger than the diamagnetic square-planar complexes. This value may indicate the presence of Ni(II) complex in mixed stereochemistry (El-Asmy et al., 1990). This interpretation is also verified by the two bands at 346 and 484 nm assignable to $^3T_1(F)\rightarrow{}^3T_1(P)$ and $^3T_1(F)\rightarrow{}^3T_2(F)$ transition, respectively compatible with the tetrahedral configuration as well as one band at 396 nm is appearing because of forbidden d–d transition, reliable with the square planar geometry of Ni(II)-complex (Saha et al., 2016).

Tauc's equation, $\alpha h\upsilon = A(h\upsilon - E_g)^r$ was used to calculate optical band gaps for Cr(III) and Ni(II) metal complexes, where (r = ø or 2 for indirect, and direct transitions, respectively), (A): energy independent constant, and (E_g): optical band gap (Hosny et al., 2020). E_g Values are estimated from the plot of ($\alpha h\upsilon$) with ($h\upsilon$) (Fig. 1). According to the curves, the direct band gaps for Cr^{3+}, and Ni^{2+} complexes are 4.64, and 4.66 eV, respectively. while, the indirect band gaps are 4.22, and 4.26 eV, respectively This information reveals that these complexes are magnetic insulators with insulating properties, high-spin frameworks, and antiferromagnetic ordering on a regular basis, i.e., metal cations in close proximity have opposite spin. Furthermore, the electronic structure of these complexes is distinguished by a predominance of metal d-orbitals in both the valence and conduction bands. (Cipriano et al., 2020).

3.5. Mass spectra

The mass spectrum of H_2L (Figure S8, Supplementary Materials) revealed that the molecular ion peak $[M]^+$ appeared at the value of m / z equal to 247, that was identical to the M. wt. of ligand. The fragmentation path of the H_2L ligand was given in Scheme 2.

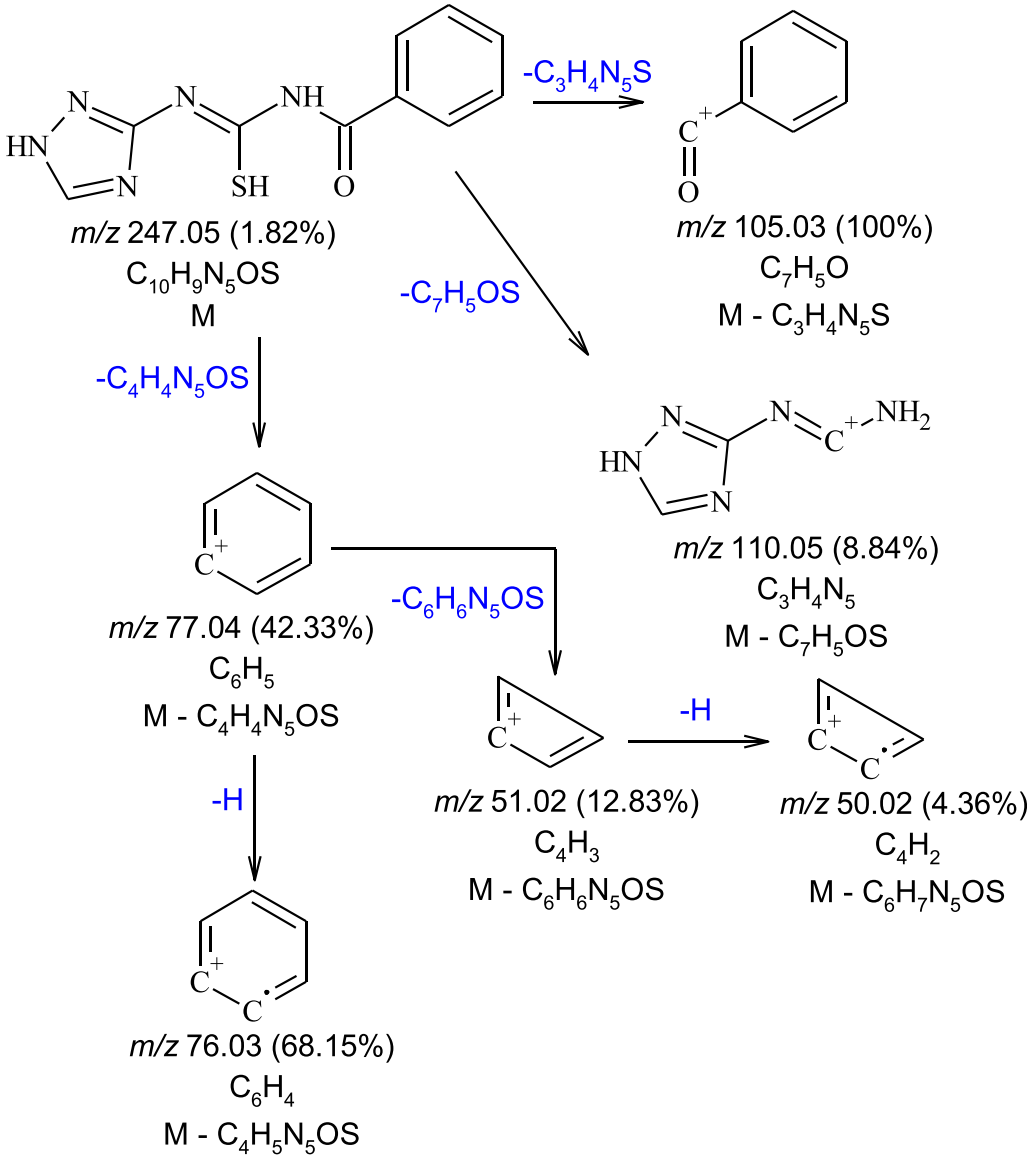

Scheme 2 The main fragments in mass spectrum of H_2L.

3.6. Photoluminescence spectra

The photoluminescence spectrum of H_2L show emission broad band at 349 nm. Moreover, its Cr(III), Ni(II) and Zn(II) complexes, show emission broad bands at 356, 349 and 359 nm, respectively, Fig. 2. These bands could be assigned to as L-M charge transfer (Singh et al., 1999; Etaiw et al., 2018). The emission bands of Cr(III) and Zn(II) complexes indicate that both are traditional blue complexes. Furthermore, the intensity of fluorescence in all complexes is substantially lower than that of free ligand. This could be because the transition metal (M)–fluorophore (F) interaction is too strong, resulting in fluorescence quenching (Zhao et al., 2010).

3.7. X ray powder diffraction of $[Ni_2(HL)Cl_2(H2O)_2].4H_2O$ complex

The XRD patterns of separated $[Ni_2(HL)Cl_2(H_2O)_2].4H_2O$ complex is depicted in Figure S9, Supplementary Materials and its (2θ)° value for peaks, the peak indexing, and interplanar spacing (d-values) were showed in Table S2, supplementary materials. The lattice parameters of Ni(II) complex has been evaluated by using match software (https://www.crystalimpact.com/match/). The $[Ni_2(HL)Cl_2(H_2O)_2].4H_2O$ complex has a triclinic space group with P −1 and lattice parameters a = 12.34 Å, b = 12.50 Å, c = 24.45 Å, α = 100.09° β = 90.31°, γ = 95.43° whose unit cell volume is 3772.94 $Å^3$. The lattice parameters of $[Ni_2(HL)Cl_2(H_2O)_2].4H_2O$ complex exhibits a good harmony with the Crystallography Open Database (COD) No. 4,332,969 (Hernández-Molina et al., 2006).

Such lattice parameters were determined by using the next relationship:

$$triclinic\ \frac{1}{d^2_{hkl}} = \left[\frac{h}{a}\begin{vmatrix}\frac{h}{a} & \cos\gamma & \cos\beta\\ \frac{k}{b} & 1 & \cos\alpha\\ \frac{l}{c} & \cos\alpha & 1\end{vmatrix} + \frac{k}{b}\begin{vmatrix}1 & \frac{h}{a} & \cos\alpha\\ \cos\gamma & \frac{k}{b} & \cos\alpha\\ \cos\beta & \frac{l}{c} & 1\end{vmatrix} + \frac{l}{c}\begin{vmatrix}1 & \cos\gamma & \frac{h}{a}\\ \cos\gamma & 1 & \frac{k}{b}\\ \cos\beta & \cos\alpha & \frac{l}{c}\end{vmatrix}\right] \cdot \begin{vmatrix}1 & \cos\gamma & \cos\beta\\ \cos\gamma & 1 & \cos\alpha\\ \cos\beta & \cos\alpha & 1\end{vmatrix}^{-1}$$

The crystalline-particle parameters were calculated using standard equations in the FWHM method (Velumani et al., 2003). the parameters were particulate sizes = 0.2897 Å lying in the nanometer scale, (2θ)° = 23.99, d spacing = 3.7102 Å, FWHM = 5.1099, the crystal strain (ε) = 1.5346 and the dislocation density (δ) = 11.9127 $Å^{-2}$. The regular-crystal lattice of the Ni(II) complex could be calculated from the minimised quantities of dislocation-density (δ) and the crystal strain (ε) (El-Metwaly et al., 2020).

3.8. Zeta potential measurements

The Zeta-potential measurements provide information regarding the stability of the colloidal suspension; the colloidal suspension is stable when the forces generating particle mutual repulsion which plays a prominent role. The higher absolute value of the zeta potential exhibits the greater the repulsion between the particles forming the suspension and thus the higher stability of suspension, whereas low values of ZP (±5 mV) indicate more flocculation between the particles and thus a higher tendency for instability (Bhagat et al., 2019). In this research, $[Ni_2(HL)Cl_2(H_2O)_2].4H_2O$ complex had the largest positive-positive repulsion with a potential of 20.3 mV suggesting the stability of this colloidal suspension. But, the ligand (H_2L) and Cr(III) complex displayed potential of −9.34 and −6.91 mV, respectively which are in the negative range, this results shows the lower stability of the suspension of the ligand (H_2L) and its Cr(III) complex. Furthermore, Zn^{2+} complex demonstrated a potential of 2.69 mV, indicating the instability of Zn(II) complex colloidal solution as the particles of this suspensions prefer to flocculate.

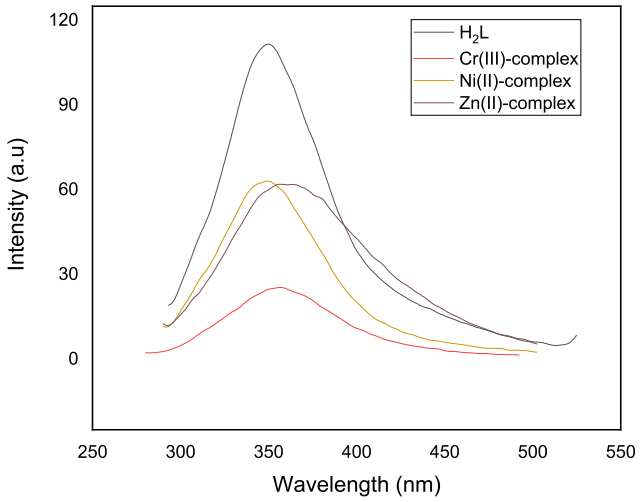

Fig. 2 Emission spectra of H_2L and its complexes in DMSO solution.

3.9. Thermogravimetric studies

Prediction of coordinated or crystallised H_2O molecules may be performed utilizing TGA data (Rakha et al., 1989; Zaky et al., 2014) (Figure S10, Supplementary Materials). It can be assumed that there is an alignment between the TGA data and the proposed molecular formula. For instance, the Cr(III) complex has 5-degradation stages. The first one seems to have a weight loss of 8.05 percent between 35 and 124 °C, suggesting the elimination of two hydrated water molecules. The step two has a weight loss of 19.67 percent in the 124–352 °C temperature range, demonstrating the elimination of the H_2O coordinating molecule and two HCl molecules. The 3rd step (from 352 to 448 °C) has a weight loss of 41.36 percent, referring to the elimination of the molecule $C_4H_3ClN_5S$. The fourth stage in the 448–547 °C range has a weight loss of 6.27 percent, relating to the elimination of C_2H_4. Finally, unoxidized carbon and metal oxide existed as a residue. Table S3, Supplementary Materials, demonstrates the steps of decomposition of complexes.

3.10. Kinetic parameters

Coats–Redfern (Coats and Redfern, 1964) and Horowitz–Metzger (Horowitz and Metzger, 1963) techniques were accustomed to predict the kinetic and thermodynamic variables of the designed complexes (Figures S11-S16, supplementary materials). Tables 3 and 4 demonstrate the various kinetic

Table 3 Kinetic Parameters of metal complexes evaluated by Horowitz-Metzger equation.

Compound	Step	Mid temp(°C)	E_a	A	ΔH*	ΔS*	ΔG*
			KJ/mol	(S^{-1})	KJ/mol	KJ/mol.K	KJ/mol
$[Cr(H_2L)Cl_3(H_2O)].2H_2O$	1st	346.25	75.34	1.53×10^{09}	72.46	−0.0703	96.82
	2nd	672.17	873.57	1.01×10^{67}	867.98	1.0311	174.92
	3rd	751.23	362.08	1.32×10^{23}	355.83	0.1900	213.10
$[Zn(HL)Cl]0.0.5H_2O$	1st	336.47	134.65	7.75×10^{18}	131.85	0.1157	92.92
	2nd	464.44	62.88	2.69×10^{04}	59.01	−0.1638	135.08
	3rd	704.58	264.67	1.67×10^{17}	258.82	0.0776	204.12
	4th	818.32	441.53	8.39×10^{25}	434.73	0.2430	235.89
$[Ni_2(HL)Cl_2(H_2O)_2].4H_2O$	1st	343.04	60.31	1.05×10^{07}	57.46	−0.1117	95.76
	2nd	505.87	78.69	3.72×10^{05}	74.48	−0.1427	146.64
	3rd	780.47	175.28	1.07×10^{09}	168.79	−0.0800	231.27

Table 4 Kinetic Parameters of metal complexes evaluated by Coats-Redfern equation.

Compound	Step	Mid temp(°C)	E_a	A	ΔH*	ΔS*	ΔG*
			KJ/mol	(S^{-1})	KJ/mol	KJ/mol.K	KJ/mol
$[Cr(H_2L)Cl_3(H_2O)].2H_2O$	1st	346.25	70.25	2.76×10^{08}	67.37	−0.0846	96.65
	2nd	672.17	841.98	3.42×10^{64}	836.39	0.9838	175.14
	3rd	751.23	350.21	2.01×10^{22}	343.97	0.1744	212.96
$[Zn(HL)Cl]0.0.5H_2O$	1st	336.47	130.86	2.08×10^{18}	128.06	0.1048	92.81
	2nd	464.44	57.66	7.82×10^{03}	53.80	−0.1741	134.64
	3rd	704.58	257.54	5.15×10^{05}	251.68	0.0679	203.86
	4th	818.32	435.60	3.61×10^{25}	428.79	0.2360	235.69
$[Ni_2(HL)Cl_2(H_2O)_2].4H_2O$	1st	343.04	54.87	1.65×10^{06}	52.02	−0.1270	95.60
	2nd	505.87	72.19	8.72×10^{04}	67.98	−0.1547	146.25
	3rd	780.47	168.13	3.83×10^{08}	161.64	−0.0886	230.79

parameters (A, E_a, ΔS*, ΔH* and ΔG*) of the separated complexes. we may notice that:

(i) A resemblance was found between the data collected from both approaches.
(ii) The good stability of the complex was proved by the high value of the activation energy.
(iii) The positive value of ΔG* shows that the degradation stage is non-spontaneous process, also, the + ve value of ΔH* suggested endothermic operations (Abu-Dief et al., 2019; Abu-Dief et al., 2020).
(iv) The negative ΔS* of certain degradation steps indicate that the activated fragments have a more orderly composition than the un-decomposed fragment and the degradation reactions become slow (Moore and Pearson, 1961). Although + ve values can indicate that the disorder of the decomposed fragments rises much faster than the un-decomposed fragment (Kenawy et al., 2001).

3.11. Molecular modeling

The optimized ligand, H_2L and its metal complexes structures that labeled with the atom symbol and its number were shown in figure S17, supplementary materials and are listed in tables S4-S11, supplementary materials. Coordination induces a minor difference in bond angles and lengths existing in the thiocarbamide structure of H_2L; the major initiatives in the angles of H_2L were N(14)-C(13)-N(11), N(15)-N(14)-C(13), S(12)-C(10)-N(8), O(9)-C(7)-N(8), O(9)-C(7)-C(7)(2), N(11)-C(10)-N(8), N(17)-C(13)-N(11), S(12)-C(10)-N(11), C(13)-N(11)-C(10), N(8)-C(7)-C(7)-C(2), and N(17)-C(13)-N(14). Analyzing the result of H_2L and the separated complexes, the following observations can be stated:

(i) As predicted, the Cr(III) structure has angles close with those predicted for octahedral complexes with sp^3d^2 hybridization (El-Gammal, 2010; El-Morshedy et al., 2019). In addition, the optimized structure of the Zn (II) complex tends to be tetrahedral (Moore and Pearson, 1961). moreover, the Ni(II) complex produced mixed geometry (tetrahedral and square planar) including sp^3 and dsp^2 hybridization.
(ii) (C = O), (C-O), (C-S), $(C = N)_{azomethine}$, and $(C = N)_{ring}$ moities have larger bond lengths than those found in the ligand (H_2L) attributed to the formation of metal–oxygen and metal-nitrogen bonds (Moore and Pearson, 1961).
i. The bond angles of coordination atoms of ligand moiety will be changed in all complexes due to the formation of chelate rings (Fukui et al., 1954).
(iii) In the Zn(II) complex, metal ion is tri-coordinated to the H_2L ligand in a tetrahedral geometry with bond angles; Cl^{19}-Zn^{18}-S^{12} = 132.55°, Cl^{19}-Zn^{18}-O^9 = 117.666°,
(iv) N(14)-Zn^{18}-O^9 = 106.487°, S^{12}-Zn^{18}-O^9 = 91.074°, N^{14}-Zn^{18}-S^{12} = 92.107° and Cl^{19}-Zn^{18}-N^{14} = 112.157° which give a small deviation from tetrahedral geometry.

3.11.1. Vibrational calculation and geometry optimization

Fig. 3 displays the computed IR spectrum of the ligand, H_2L in the vacuum and its observed spectrum. A slight variation between the observed and the computed can be found since the observed spectrum was evaluated for the solid material. Figure S18, Supplementary Materials is the relationship chart between the computed and the observed wavenumbers demonstrate the linear relationship according to the given equation $\nu_{cal} = 0.878\ \nu_{Exp} + 119.321$ whereas $R^2 = 0.9866$.

By the aid of Density functional theory (DFT), we have been able to determine different quantum variables as E_{LUMO}, E_{HOMO}, dipole moment, binding energy, and compounds' total energy (Table 5) (Liu et al., 2012; Yousef et al., 2012; Govindarajan et al., 2012; Abu El-Reash et al., 2013; Pearson, 1989; Padmanabhan et al., 2007; Gaber et al., 2018). Figure S19, supplementary materials includes the energy of frontier molecular orbitals (FMOs, that includes both orbitals of HOMO and LUMO). The data designated that:

(i) the stability of studied metal complexes was demonstrated by the high E_a value and it was verified by the negative E_{HOMO} and E_{LUMO} value (Gaber et al., 2018; Abu El-Reash et al., 2013).

(ii) Generally, the HOMO orbital was dispersed on O(9), S (12), N(8), N(11), N(15), N(14), and N(17) atoms, which are the expected position for nucleophilic attacks in the metal ion.

(iii) The stability of metal complexes than the ligand, H_2L has been explained from the total energy measurements (Aljahdali and El-Sherif, 2013).

3.11.2. Molecular electrostatic potential (MEP) of H_2L

Physical and electrostatic potential behavior is estimated by the theoretical or diffraction strategies. MEP was expressed based on electronic density (Zalaoglu et al., 2010) since has been used as a parameter in the description of nucleophilic and electrophilic attack locations and also the interaction of hydrogen bonds. Figure S20, Supplementary Materials shows the MEP which illustrated for the compounds in the study that shows that the greenish color region pointed to the neutral electrostatic potential field, whereas the blue region is the favored position for the nucleophilic attack that had the lowest zone of e's (Tanak et al., 2011). However, the reddish color section related to the region rich in e's as well as the position needed for electrophilic attack.

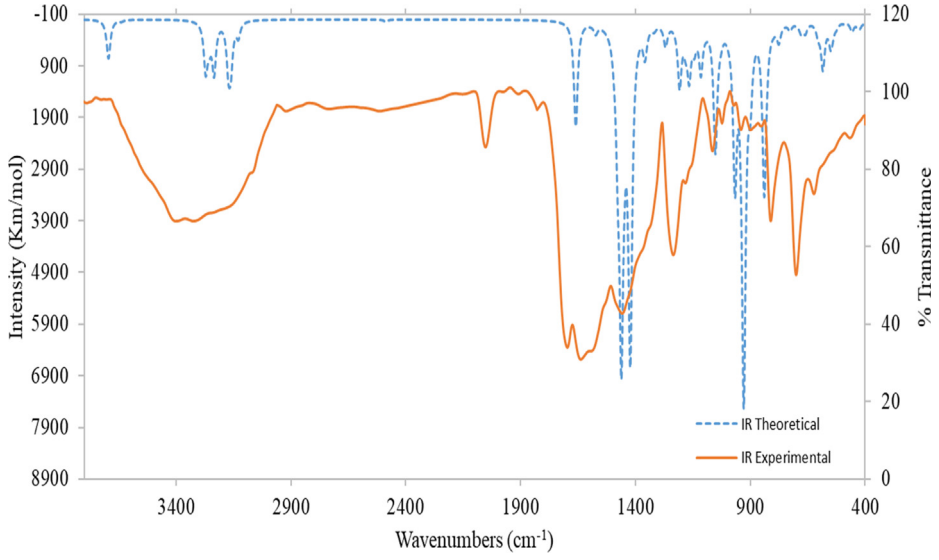

Fig. 3 Comparison of experimental and theoretical IR spectra of Ligand (H_2L).

Table 5 Calculated gas phase energy, dipole moment, E_{HOMO}, E_{LUMO}, energy band gap ($E_H - E_L$), chemical potential (μ), electronegativity (χ), global hardness (η), global softness (S) and global electrophilicity index (ω) for ligand and its complexes.

Compound	E_H (eV)	E_L (eV)	(E_H -E_L) (eV)	χ (eV)	μ (eV)	η (eV)	S (eV^{-1})	(ω) (eV)	σ (eV)	dipole moment (debye)	Total Energy kcal/mol
H_2L	−5.271	−2.377	−2.894	3.824	−3.824	1.447	0.724	5.053	0.691	3.451	-7.12×10^{05}
Cr(III)-Complex	−4.435	−2.857	−1.578	3.646	−3.646	0.789	0.395	8.424	1.267	9.818	-1.69×10^{06}
Ni(II)-Complex	−4.294	−4.083	−0.211	4.189	−4.189	0.106	0.053	83.145	9.479	8.447	-1.63×10^{06}
Zn(II)-Complex	−5.374	−3.498	−1.876	4.436	−4.436	0.938	0.469	10.489	1.066	2.767	-1.16×10^{06}

(E_H, E_L): Frontier molecular orbitals energies of HOMO and LUMO, (E_H -E_L): energy band gap, (χ): electronegativity, (S): global softness, (μ): chemical potential, (η): global hardness, (ω) global electrophilicity index and (σ): softness.

3.11.3. Mulliken population analysis of H_2L

Mulliken atomic charge has a major part to play in the mathematical interpretation of the molecular construction. Figure S21, Supplementary Materials and Tables S12-S15, Supplementary Materials show the distribution of charges of H_2L, while oxygen and nitrogen atoms provide a negative value, however most carbons and hydrogens atoms provide positive values. This may be due to the e-donating potential of oxygen and nitrogen atoms.

3.12. Catalytic degradation of azo dye

The catalytic activity of [Zn(HL)Cl]0.0.5H_2O complex was investigated in the oxidative degradation of an organic dye, such as EBT dye, using H_2O_2 as the oxidizing agent "due to its green character". The oxidation did not occur in the absence of the H_2O_2 or Zn(II) catalyst, but when both oxidant and catalyst were used, the dye degraded. As a result, the impact of H_2O_2 dose was studied in combination with the impact of time and temperature to determine the ideal conditions for the reaction. The effect of time was investigated at a constant dose of H_2O_2 (0.2 ml) and constant dye concentration (30 ppm) by running the reaction for 5-, 10-, 15-, 20-, and 30-minute intervals. Early, the effect of temperature was investigated by performing the reaction at room temperature (30℃), 45, and 60℃. Finally, the effect of H_2O_2 dose was investigated by using 0.2, 0.3, 0.4, 0.5, and 0.6 ml of H_2O_2 and constant dye concentration and temperature (30 ppm, and 30 ℃, respectively). The results of the experiment are shown in (Fig. 4), which shows that the degradation of the dye increases with the time of the reaction, with about 45 percent of the dye removed after 30 min. By increasing the H_2O_2 dose, the degradation first improved and then began to be constant or decrease, as shown by self-quenching of OH radicals according to the succeeding OH equation:

$$H_2O_2 + OH \rightarrow H_2O + HO_2$$

$$HO_2 + OH \rightarrow H_2O_2 + O_2$$

After 10 min, at a constant dose of H_2O_2 (0.2 ml) and constant dye concentration, the effect of temperature on the reaction was investigated (30 ppm). The study indicate that the capacity of dye removal increases with temperature, with only 57 percent of the dye remaining after 10 min at 60 °C compared to 85 percent at 30 °C.

3.13. Potentiometric studies

3.13.1. Protonation constants of ligand (L)

Table 6 shows the stoichiometric protonation constants of the investigated Ligand (L). The ligand compound investigated here has two protonation constants, corresponding to the protonated N-triazol ring and C-SH groups. As shown in Scheme 3, the N-triazol ring has the highest pKa value (pK_{a1} = 8.60, at 25 °C) and the Sulphur group has the lowest (pK_{a2} = 4.74, at 25 °C). Fig. 5 depicts the species distribution of the ligand (L). The ligand (L^{2+}) from Sulphur group to form HL^+ tends to lose it protons after the pH is raised to the pH range of 4.71–4.74. As the conditions become more

Table 6 Stability constants of Ni(II)- L in 50% (V/V) Dioxane-Water at different temperatures and I = 0.05 M KCl.

System	*T*(°C)	$\log_{10}\beta$
L	25	8.60
		13.34
	35	8.54
		13.27
	45	8.52
		13.23
Ni- L	25	8.60
		13.40
	35	8.56
		13.35
	45	8.25
		13.02

L: (Z)-N-benzoyl-N'-(1H-1,2,4-triazol-3-yl)carbamimidothioic acid.

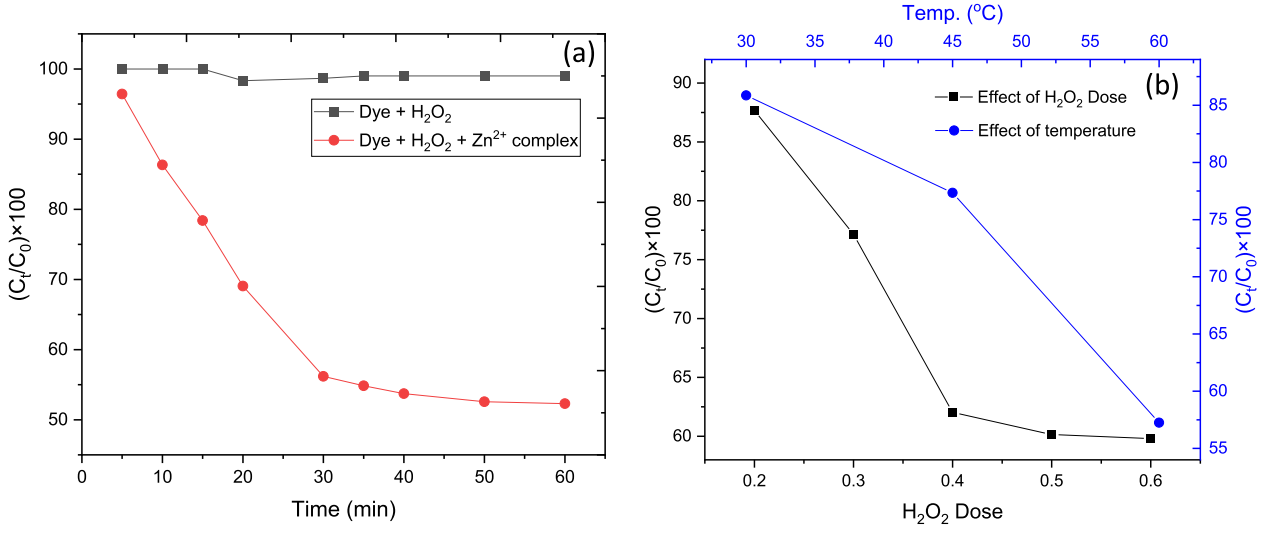

Fig. 4 (a) Effect of time on catalytic degradation, and (b) Dye removal against temperature and H_2O_2 dose.

alkaline, the second proton aims to be deprotonated to a free ligand (L).

3.13.2. Stability constants of the Ni-L complexes

The stability constants of binary chelated ligand (L) with Ni (II) metal ion as an example of divalent transition metal ions. The comparison of the titration curves of free ligand with the complexed ligand shows that adding Ni(II) ion to the free ligand solution lowers the pH. As a result, the curves associated with complexes are found at lower pHs than that of the free ligand because they require more alkali to raise the pH to the level of the free ligand. The release of protons from the coordinated ligand is an implication of complex formation. The stoichiometric stability constants associated with the inspected ligand's Ni(II) complex were estimated in 50 % (V/V) Dioxane-Water at various temperatures and are shown in Table 6.

Table 6 shows the logarithms of the stability constants for all complex systems evaluated by potentiometric equilibrium titration process (1) and (2) (simplicity charges are omitted):

$$M + L \rightleftharpoons ML\beta = \frac{[ML]}{[M][L]} \quad (1)$$

$$M + 2L \rightleftharpoons ML_2\beta = \frac{[ML_2]}{[M][L]^2} \quad (2)$$

The Ni-L process distribution diagram (Fig. 6) is investigated with the goal of investigating the changes in concentration of the Ni(II) complex with pH. The Ni-L complex is generated at pH 5.5 with a maximum of 95 %, while at pH 8, the complex $Ni(L)_2$ is formed.

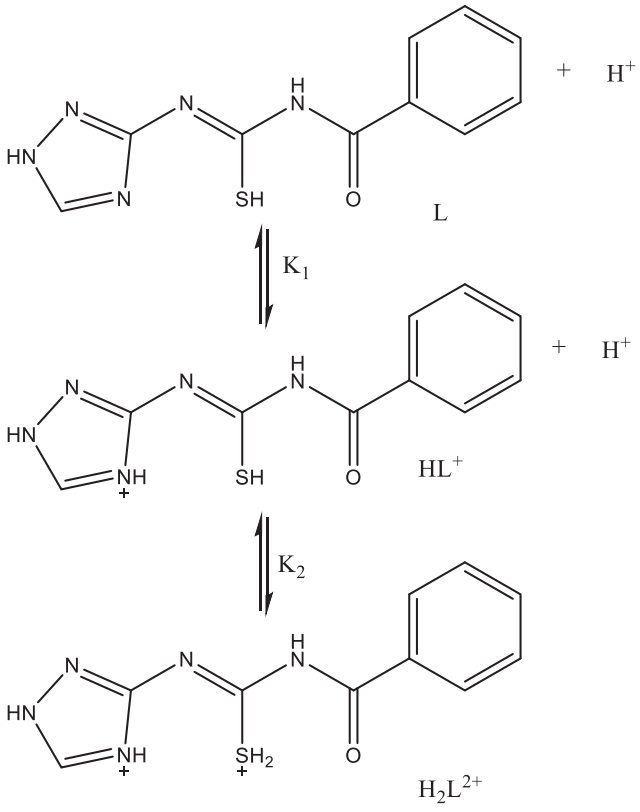

Scheme 3 Protonation process of Ligand.

3.13.3. Effect of temperature and thermodynamics

The protonation of the ligand and its Ni^{2+} complex is attributed to the data of thermodynamic parameters that are relative to the temperature data shown in Tables 7 and 8. ΔS and ΔH values were determined by establishing a correlation between equilibrium constant values (ln K) and temperature reciprocal values (1/T) ($\ln K = -\Delta H/RT + \Delta S/R$) resulting in an intercept ΔS/R, and a slope –ΔH/R (Figs. 7 and 8). There are several conclusions, which are summarized below:

a. The reaction involving ligand protonation is exothermic and has a net negative ΔG (Table 7).

b. The data in Table 8 show that the values of $\log_{10} K_1$ - $\log_{10} K_2$ for binary complexes are positive, implying that the first ligand molecule coordinates to the metal ion is preferable to its bonding to the second (El-Sherif et al., 2012). This may demonstrate the significance of the steric effects caused by the addition of the second molecule of the ligand i.e., the NiL_2 (1:2) species cannot be formed until the NiL(1:1) species is

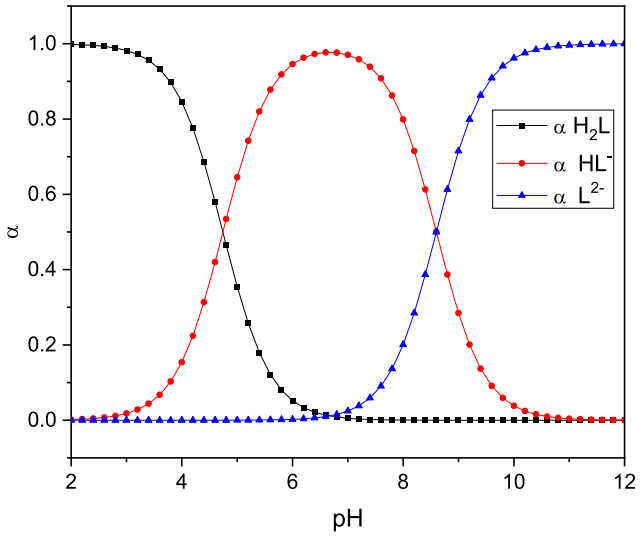

Fig. 5 Species distribution of the ligand (L).

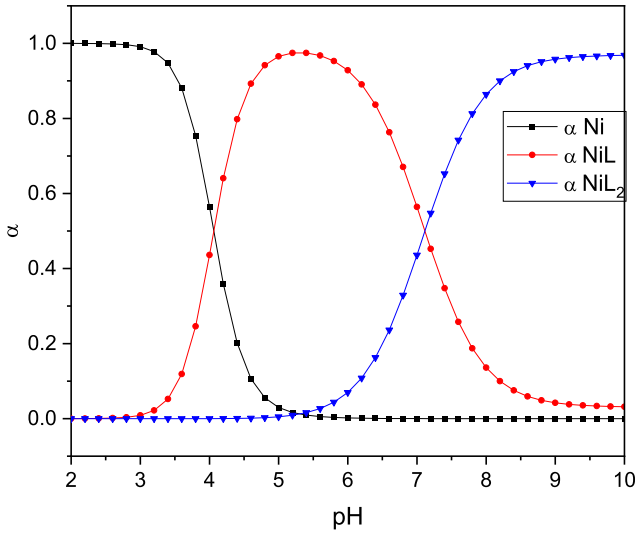

Fig. 6 Species distribution of the Ni(II)-L complex.

Table 7 Protonation constants of L in 50% (V/V) Dioxane-Water at different temperatures and I = 0.05 M KCl.

T(°C)		pK	Thermodynamic parameters		
			ΔH^o kJ mol^{-1}	ΔS^o JK^{-1} mol^{-1}	ΔG^o kJ mol^{-1}
25	$L + H^+ \rightleftharpoons HL^+$	8.60			
35		8.54	−7.2949	0.14008	−50.4395
45		8.52			
25	$HL^+ + H^+ \rightleftharpoons L^{+2}$	4.74			
35		4.73	−2.7111	0.08169	−27.8744
45		4.71			

Table 8 Stepwise stability constants of Ni- L in 50% (V/V) Dioxane-Water at different temperatures and I = 0.05 M KCl.

T(°C)		pK	Thermodynamic parameters		
			ΔH^o kJ mol^{-1}	ΔS^o JK^{-1} mol^{-1}	ΔG^o kJ mol^{-1}
25	$Ni + L \rightleftharpoons NiL$	8.60			
35		8.56	−31.4787	0.05991	−49.9307
45		8.25			
25	$NiL + L \rightleftharpoons NiL_2$	4.8			
35		4.79	−2.6856	0.08285	−28.2027
45		4.77			

formed. This could be due to: (i) an improvement in free metal ion Lewis acidity (M^{+n}) when compared to a 1:1 chelated ion ($ML^{+\ n-1}$) and (ii) steric weakness resulting from the addition of a 2nd bulky ligand to the chelated ion $ML^{+\ n-1}$.

c. All of the negative values correlated with the complex formation of the Gibb free energy reflect the random existence of the Ni-L complex formation reactions.

d. The negative heat content (ΔH) values indicate that the complex formation operation is exothermic, implying that the chelation operation works better at low temperatures.

e. The ligand complex (ΔS) values are positive, suggesting that the metal complex formation is entropically favorable (El-Sherif and Eldebss, 2011), and the complexation mechanism is related to the production of hydrogen ion (H^+) and H_2O molecules (Jeragh et al., 2007). During the production of metal chelates, the ligand displaces water molecules from the metal ion's main hydration sphere. The number of particles in the process thus increases, implying that the system's randomness increases with the next equation.

$$\left[M(H_2O)_n\right]^{2+}_{(aq)} + L^-_{(aq)} \rightleftharpoons ML^+_{(aq)} + nH_2O$$

f. indicate that the complexation mechanism is spontaneous and exothermic, implying that the process of complex formation is entropically favorable.

It can be concluded that log K_1 > log K_2 indicates that Ni (II) ion empty locations are more readily available for binding the 1st ligand than the 2nd one. The chelation mechanism-

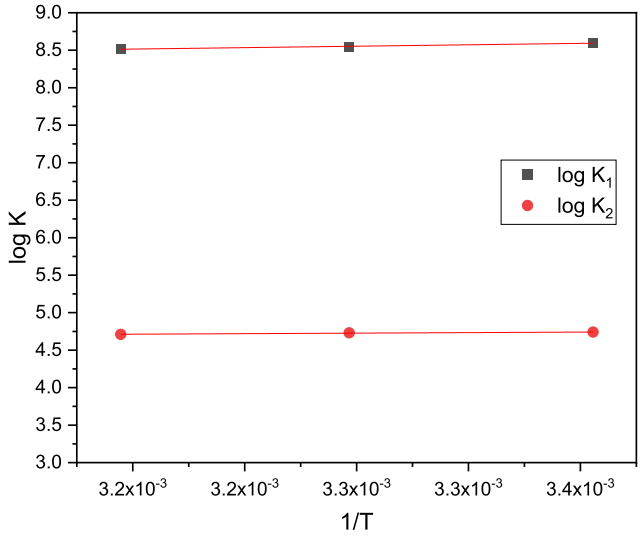

Fig. 7 Effect of temperature on the dissociation constant of ligand (L).

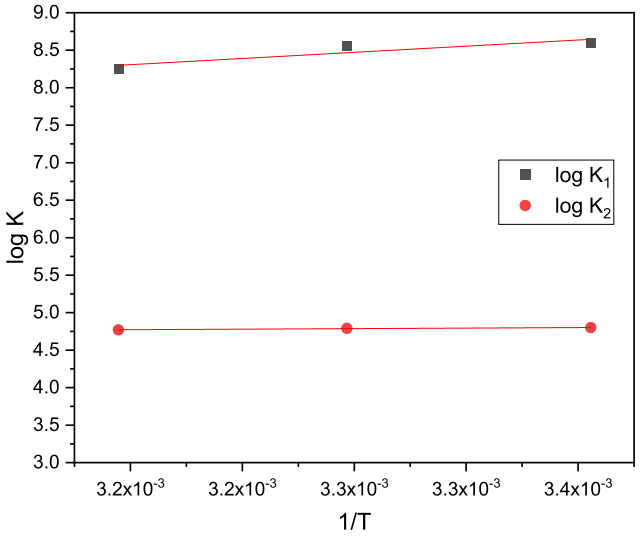

Fig. 8 Effect of temperature on the formation constants of Ni (II)– L complex.

Table 9 Antibacterial and antifungal of ligand (H_2L) and its metal complexes.

Sample		Inhibition zone diameter (mm/mg Sample)			
		Bacteria		Fungi	
		Escherichia coli) G^-)	*Staphylococcus aureus*) G^+)	*Aspergillus flavus* (Fungus)	*Candida albicans* (Fungus)
Standard	Ampicillin: Antibacterial agent	25 ± 1.2	21 ± 1.6	–	–
	Amphotericin B: Antifungal agent	–	–	16 ± 2.5	19 ± 1.4
Control: DMSO		0.0	0.0	0.0	0.0
H_2L		15 ± 1.4	13 ± 2.1	0.0	19R ± 2.1
$[Cr(H_2L)Cl_3(H_2O)].2H_2O$		16.0 ± 2.3	15.0 ± 1.8	0.0	11.0 ± 3.2
$[Ni_2(HL)Cl_2(H_2O)_2].4H_2O$		14.0 ± 1.5	10.0 ± 1.3	0.0	15R ± 1.6
$[Zn(HL)Cl]0.0.5H_2O$		13.0 ± 2.6	19R ± 2.4	0.0	0.0

G: Gram reaction.
Solvent: DMSO.
R: Repellent action (not complete inhibition).

induced reaction is exothermic, spontaneous, and entropically favorable.

3.14. Biological studies

3.14.1. Antimicrobial activity

The antimicrobial effects of the Schiff base ligand and metal complexes were undertaken toward *S. aureus*, *C. Albicans*, *E. coli* and *A. flavus* (Table 9), while Amphotericin B and Ampicillin were being used as guideline for anti-fungal and antibacterial behavior, respectively. The Cr(III) complex displayed the highest inhibitory effect towards all microorganisms under investigation based on the estimated area diameter (mm/mg Sample). In addition, all compounds were evaluated no action against *A. flavus* fungus stain. Also, the Zn(II) complex did not show any activity against those fungus stain. Various antibacterial potency can be due to variations in the composition of the cell wall of the microorganisms (Koch, 2003).

3.14.2. ABTS-antioxidant activity

All prepared compounds have been evaluated for ABTS-antioxidant behavior Table 10. Ni(II) complex displayed significant antioxidant potency with percent inhibition = 70.50% relative to ascorbic acid. Whereas ligand, H_2L and other M^{2+}-complexes exhibited moderate potency.

3.14.3. The cytotoxicity of H_2L and its metal complexes

2-various cell lines, HePG2 (liver carcinoma), and MCF-7 (breast carcinoma), have been used to determine the cytotoxicity of the prepared compounds under investigation (*in vitro*). The represented Fig. 9 demonstrates the relationship between concentration and cell viability. By such plots, IC_{50} values (IC_{50} is the concentration that inhibits 50 percent) can be determined as shown in Table 11. The results may be summarized in the following points:

a. The Ni(II)-complex demonstrates effective strong activity towards MCF-7 and HePG2 cells with IC_{50} values of 10.96 ± 1.0 and 8.31 ± 0.9 μM, respectively, identifying that Ni(II) complex acts as chemo-therapeutically substantial (Yousef et al., 2014).

Table 10 ABTS antioxidant of ligand (H_2L) and its metal complexes.

Compounds	Absorbance of samples	% inhibition
Control of ABTS	0.546	0%
Ascorbic-acid	0.059	89.2%
H_2L	0.403	26.2%
$[Cr(H_2L)Cl_3(H_2O)].2H_2O$	0.413	24.3%
$[Ni_2(HL)Cl_2(H_2O)_2].4H_2O$	0.161	70.5%
$[Zn(HL)Cl]0.0.5H_2O$	0.416	23.8%

b. Cr(III)-complex exhibited moderate activity toward MCF-7 and HePG2 cell lines with IC_{50} values 41.03 ± 2.9 and 27.71 ± 2.1 μM, respectively.
c. The weak action of Zn(II) complex towards both cancer cells with IC_{50} = 54.30 ± 3.5 and 61.97 ± 3.7 μM.
d. Finally, H_2L exhibited weak action towards HePG2 cancer cells with IC_{50} values equal to 54.14 ± 3.3 μM and also moderate potency towards MCF-7 cancer cells with IC_{50} values 33.82 ± 2.5 μM.

3.15. Molecular docking with EGFR protein

It is believed that molecular binding is very important in drug discovery. The investigated compounds related to the most suitable active site of 3W2S of EGFR (PHE 856, LYS 745, ASP 855, CYS 797, ARG 841, ASN 842, MET 793, LEU 718, GLY 719, SER 720, VAL 726, ASP 800, and PHE 997) that predicted by the site-finder algorithm in MOE (Fig. 10 and Figures S22-S24). The largest binding pocket was assigned and all hits were docked against the most active site using the MOE docking software, Table 12. As a glance in this table, the S values of investigated compounds are close to each other. Thus, the inhibitory activity may be compared according to the type and number of interaction bonds of the tested compounds with EGFR protein. According to the interaction with EGFR, the inhibitory activity order is $[Ni_2(HL)Cl_2(H_2O)_2].4H_2O$ > H_2L > $[Cr(H_2L)Cl_3(H_2O)].2H_2O$ > $[Zn(HL)Cl]0.0$.

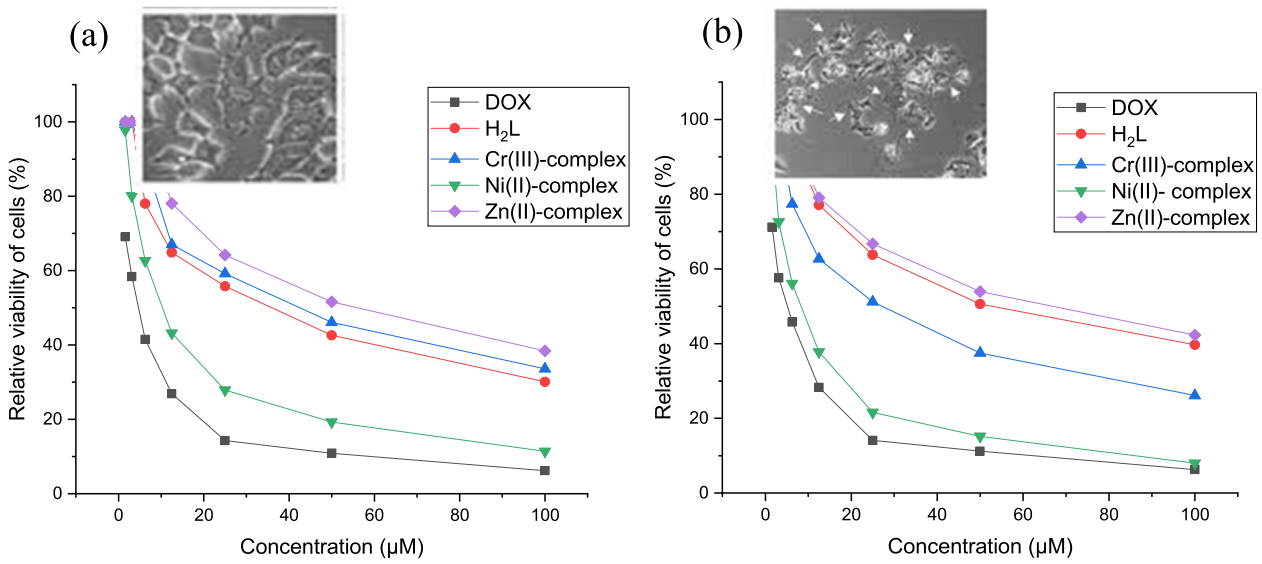

Fig. 9 In vitro antitumor activity of Doxorubicin, H2L and isolated compounds against (a) breast cancer (MCF7) (b) liver carcinoma (HePG2).

Table 11 Cytotoxic activity of ligand (H_2L) and its metal complexes against human tumor cells.

Compounds	In vitro Cytotoxicity IC_{50} (μM)	
	HePG2	MCF-7
DOX	4.50 ± 0.3	4.17 ± 0.2
H_2L	54.14 ± 3.3	33.82 ± 2.5
$[Cr(H_2L)Cl_3(H_2O)].2H_2O$	27.71 ± 2.1	41.03 ± 2.9
$[Ni_2(HL)Cl_2(H_2O)_2].4H_2O$	8.31 ± 0.9	10.96 ± 1.0
$[Zn(HL)Cl]0.0.5H_2O$	61.97 ± 3.7	54.30 ± 3.5

DOX: Doxorubicin.
IC_{50} (μM): 1 – 10 (very strong). 11 – 20 (strong). 21 – 50 (moderate). 51 – 100 (weak) and above 100 (non-cytotoxic) (El-Sayed et al., 2018).

$5H_2O$. This order is harmonious with experimental data. It has been observed that the contact between H-donor and H-acceptor is the most common type of interaction with EGFR receptor while Zn(II)-complex doesn't show any interactions with EGFR receptor. Based on the results tabulated, it can be deduced that the Ni(II)-complex (Figure S23, Supplementary Materials) has the highest inhibitory activity of the EGFR protein which is similar to experimental data. In this complex, two nitrogen atoms of ligand build two H-acceptor interactions with LYS 745 and LEU 858 of EGFR (with distances 2.70 and 3.49 Å) also oxygen atoms of water molecules build two H-donor interactions with ASP 837 and ASN 842 of EGFR (with distances 2.52 and 2.98 Å). While in EGFR-H_2L interaction (Fig. 10), there is one H-donor and one H-acceptor interactions with nitrogen and oxygen atoms with

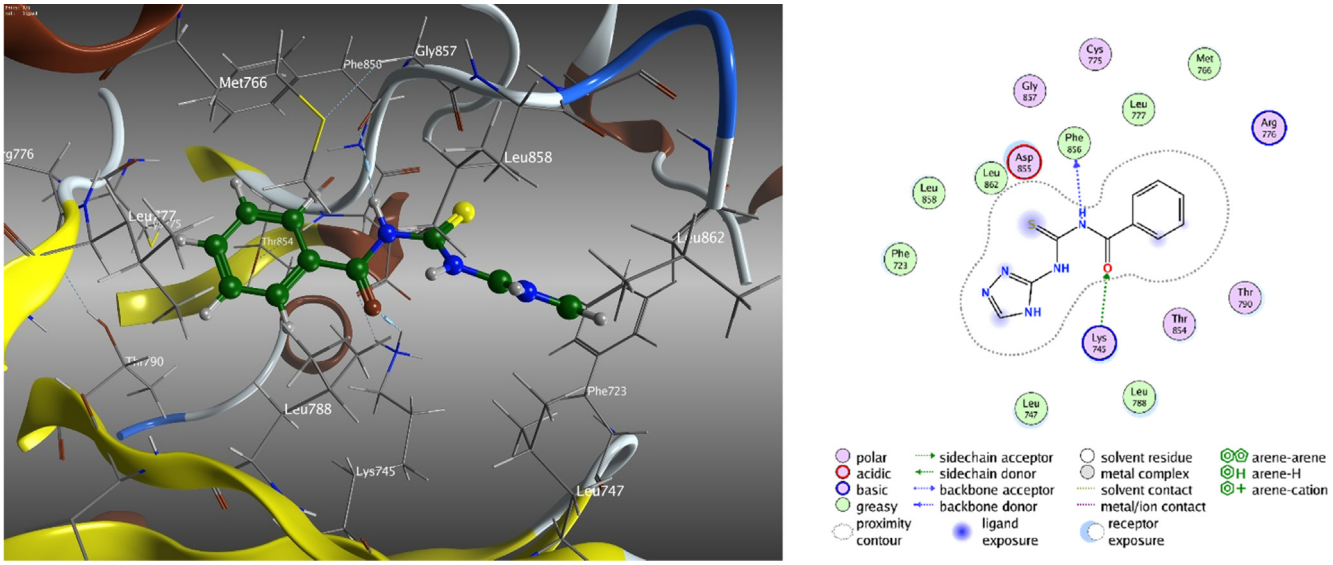

Fig. 10 3D and 2D molecular interaction of ligand, H_2L to inhibitory activity to the EGFR protein.

Table 12 Molecular docking scoring, RMSD, interaction results of the investigated compounds.

Compounds	S	RMSD	interaction	Receptor	Distance (Å)
H_2L	−6.27324	0.72187	H-donor H-acceptor	PHE 856 LYS 745	3.21 2.96
$[Cr(H_2L)Cl_3(H_2O)].2H_2O$	−4.87598	1.421159	π-cation	LYS 745	4.01
$[Ni_2(HL)Cl_2(H_2O)_2].4H_2O$	−5.54184	1.219244	H-donor H-donor H-acceptor H-acceptor	ASP 837 ASN 842 LYS 745 LEU 858	2.52 2.98 2.70 3.49
$[Zn(HL)Cl]0.0.5H_2O$	−5.14431	1.180049	———	———	———

PHE 856, and LYS 745, respectively (with distances 3.21 and 2.96 Å). Finally, Cr(III)- complex shows only π-cation interaction of five-membered ring of ligand with LYS 745 of EGFR (distance = 4.01 Å).

4. Conclusion

In the present manuscript, a new thiocarbamide derivative (H_2L), was produced by the reaction of benzoyl isothiocyanate with 3-amino triazole. Its Cr(III), Ni(II) and Zn(II) complexes were synthesized and characterized using various spectroscopic techniques. The ligand operates as a neutral bidentate, mononegative tridentate and binegative tetradentate in the Cr(III), Zn(II) and Ni(II) complexes, respectively. The photoluminescence spectra of ligand and its metal complexes exhibits that fluorescence quenching of complexes than free ligand. The suggested frameworks of these complexes have been optimized using the DFT analysis. Coats-Redfern and Horowitz-Metzger methods have been used to calculate the kinetic parameters (Ea, A, ΔH*, ΔS* and ΔG*) for titled complexes of all thermal degradation stages. The catalytic activity The Zn(II) complex demonstrated promising activity in the degradation of organic dyes, indicating that it can be used as a starting point for developing catalysts in such features. The greater cytotoxicity and ABTS-antioxidant activity were observed in the Ni(II) complex relative to the other studied compounds. Whereas Cr(III) complex exhibits the highest antimicrobial activity towards *E. coli, S. aureus* and *C. albicans*. According to molecular docking interaction, Ni(II) complex exhibits the highest inhibitory activity to the EGFR protein that agree with the experimental anticancer data.

Declaration of Competing Interest

The authors declare that they have no known competing financial interests or personal relationships that could have appeared to influence the work reported in this paper.

Acknowledgment

I wish to thank Dr. Mohammed M. El-Gamil, expert of Toxic and Narcotic Drug, Forensic Medicine, Ministry of Justice, Egypt for his help in preparing metal complexes and for his instructions for theoretical studies.

Appendix A. Supplementary material

Supplementary data to this article can be found online at https://doi.org/10.1016/j.arabjc.2022.104104.

References

Abbas, S.Y., Al-Harbi, R.A., El-Sharief, M.A.S., 2020. Synthesis and anticancer activity of thiourea derivatives bearing a benzodioxole moiety with EGFR inhibitory activity, apoptosis assay and molecular docking study. Eur. J. Med. Chem. 198,. https://doi.org/10.1016/j.ejmech.2020.112363 112363.

Abdel-Monem, Y.K., Abouel-Enein, S.A., 2017. Structural, spectral, magnetic and thermal studies of 5-(thiophene-2-ylmethine azo) uracil metal complexes. J. Therm. Anal. Calorimet. 130 (3), 2257–2275. https://doi.org/10.1007/s10973-017-6507-x.

Abdel-Monem, Y.K., Abouel-Enein, S.A., El-Seady, S.M., 2018. Synthesis, characterization and molecular modeling of some transition metal complexes of Schiff base derived from 5-aminouracil and 2-benzoyl pyridine. J. Mol. Struct. 1152, 115–127. https://doi.org/10.1016/j.molstruc.2017.09.038.

L.H. Abdel-Rahman, A.M. Abu-Dief, R.M. El-Khatib, S.M. Abdel-Fatah, Some new nano-sized Fe(II), Cd(II) and Zn(II) Schiff base complexes as precursor for metal oxides: Sonochemical synthesis, characterization, DNA interaction, in vitro antimicrobial and anticancer activities, Bioorg. Chem. 69 (2016) 140-152. https://doi.org/10.1016/j.bioorg.2016.10.009.

Abdel-Rhman, M.H., Hussien, M.A., Mahmoud, H.M., Hosny, N.M., 2019. Synthesis, characterization, molecular docking and cytotoxicity studies on N-benzyl-2-isonicotinoylhydrazine-1-carbothioamide and its metal complexes. J. Mol. Struct. 1196, 417–428. https://doi.org/10.1016/j.molstruc.2019.06.092.

Abu El-Reash, G.M., El-Gammal, O.A., El-Gamil, M.M., 2013. Structural, spectral, DFT, pH-metric and biological studies on Cr (III), Mn(II) and Fe(III) complexes of dithione heterocyclic thiosemicarbazide ligand. Spectrochim. Acta, A104, 383–393. https://doi.org/10.1016/j.saa.2012.11.070.

Abu El-Reash, G.M., El-Gammal, O.A., Ghazy, S.E., Radwan, A.H., 2013. Characterization and biological studies on Co (II), Ni (II) and Cu (II) complexes of carbohydrazones ending by pyridyl ring. Spectrochim. Acta, A 104, 26–34. https://doi.org/10.1016/j.saa.2012.11.008.

Abu-Dief, A.M., Abdel-Rahman, L.H., Shehata, M.R., Abdel-Mawgoud, A.A.H., 2019. Novel azomethine Pd (II)- and VO (II)-based metallo-pharmaceuticals as anticancer, antimicrobial, and antioxidant agents: design, structural inspection, DFT investigation, and DNA interaction. J. Phys. Org. Chem. 32, (12). https://doi.org/10.1002/poc.4009 e4009.

Abu-Dief, A.M., Abdel-Rahman, L.H., Abdelhamid, A.A., Marzouk, A.A., Shehata, M.R., Bakheet, M.A., Almaghrabi, O.A., Nafady, A., 2020. Synthesis and characterization of new Cr(III), Fe(III) and Cu(II) complexes incorporating multi-substituted aryl imidazole ligand: structural, DFT, DNA binding, and biological implications. Spectrochim. Acta, A 228,. https://doi.org/10.1016/j.saa.2019.117700 117700.

Abu-Dief, A.M., El-khatib, R.M., Sayed, S.M.E., Alzahrani, S., Alkhatib, F., El-Sarrag, G., Ismael, M., 2021. Tailoring, structural elucidation, DFT calculation, DNA interaction and pharmaceutical applications of some aryl hydrazone Mn(II), Cu(II) and Fe(III)

complexes. J. Mol. Struct. 1244,. https://doi.org/10.1016/j.molstruc.2021.131017 131017.

Abu-Dief, A.M., El-khatib, R.M., Aljohani, F.S., Alzahrani, S.O., Mahran, A., Khalifa, M.E., El-Metwaly, N.M., 2021. Synthesis and intensive characterization for novel Zn(II), Pd(II), Cr(III) and VO(II)-Schiff base complexes; DNA-interaction, DFT, drug-likeness and molecular docking studies. J. Mol. Struct. 1242,. https://doi.org/10.1016/j.molstruc.2021.130693 130693.

A.M. Abu-Dief, L.H. Abdel-Rahman, M.A. Abd-El Sayed, M.M. Zikry, A. Nafady, Green Synthesis of AgNPs Ultilizing Delonix Regia Extract as Anticancer and Antimicrobial Agents**, ChemistrySelect 5(42) (2020) 13263-13268. https://doi.org/10.1002/slct.202003218.

Aeschlach, R., Loliger, J., Scott, C.B., Murcia, A., Butler, J., Halliwel, B., Aruoma, I.O., 1994. Antioxidant actions of thymol, carvacrol, 6-gingerol, zingerone and hydroxytyrosol. Food Chem. Toxicol. 32, 31–36. https://doi.org/10.1016/0278-6915(84)90033-4.

Aljahdali, M., El-Sherif, A.A., 2013. Synthesis, characterization, molecular modeling and biological activity of mixed ligand complexes of Cu (II), Ni (II) and Co (II) based on 1, 10-phenanthroline and novel thiosemicarbazone. Inorg. Chim. Acta 407, 58–68. https://doi.org/10.1016/j.ica.2013.06.040.

Aljohani, E.T., Shehata, M.R., Abu-Dief, A.M., 2021. Design, synthesis, structural inspection of Pd2+, VO2+, Mn2+, and Zn2+ chelates incorporating ferrocenyl thiophenol ligand: DNA interaction and pharmaceutical studies. Appl. Organomet. Chem. 35, (4). https://doi.org/10.1002/aoc.6169 e6169.

Alkhamis, K., Alsoliemy, A., Aljohani, M.M., Alrefaei, A.F., Abumelha, H.M., Mahmoud, M.H.H., Zaky, R., El-Metwaly, N., 2021. Conductometry of nano-sized zinc sulfate; synthesis and characterization of new hydrazone complexes: conformational and in-vitro assay. J. Mol. Liq. 340,. https://doi.org/10.1016/j.molliq.2021.117167 117167.

Almalki, S.A., Bawazeer, T.M., Asghar, B., Alharbi, A., Aljohani, M. M., Khalifa, M.E., El-Metwaly, N., 2021. Synthesis and characterization of new thiazole-based Co(II) and Cu(II) complexes; therapeutic function of thiazole towards COVID-19 in comparing to current antivirals in treatment protocol. J. Mol. Struct. 1244,. https://doi.org/10.1016/j.molstruc.2021.130961 130961.

Al-Qahtani, S.D., Alsoliemy, A., Almehmadi, S.J., Alkhamis, K., Alrefaei, A.F., Zaky, R., El-Metwaly, N., 2021. Green synthesis for new Co(II), Ni(II), Cu(II) and Cd(II) hydrazone-based complexes; characterization, biological activity and electrical conductance of nano-sized copper sulphate. J. Mol. Struct. 1244,. https://doi.org/10.1016/j.molstruc.2021.131238 131238.

Anliker, R., 1979. Ecotoxicology of dyestuffs—a joint effort by industry. Ecotoxicol. Environ. Saf. 3 (1), 59–74. https://doi.org/10.1016/0147-6513(79)90060-5.

Avdović, E.H., Milanović, Ž.B., Živanović, M.N., Šeklić, D.S., Radojević, I.D., Čomić, L.R., Trifunović, S.R., Amić, A., Marković, Z.S., 2020. Synthesis, spectroscopic characterization, biological activity, DFT and molecular docking study of novel 4-hydroxycoumarine derivatives and corresponding palladium (II) complexes. Inorg. Chim. Acta 504,. https://doi.org/10.1016/j.ica.2020.119465 119465.

Bhagat, M., Anand, R., Datt, R., Gupta, V., Arya, S., 2019. Green synthesis of silver nanoparticles using aqueous extract of Rosa brunonii Lindl and their morphological, biological and photocatalytic characterizations. J. Inorg. Organomet. Polym. 29 (3), 1039–1047. https://doi.org/10.1007/s10904-018-0994-5.

N. Chubar, J.R. Carvalho, M.J.N. Correia, Cork biomass as biosorbent for Cu (II), Zn (II) and Ni (II), Colloids Surf., A 230(1) (2003) 57-65. https://doi.org/10.1016/j.colsurfa.2003.09.014.

Chung, K.-T., Stevens Jr., S.E., 1993. Degradation azo dyes by environmental microorganisms and helminths. Environ. Toxicol. Chem. 12 (11), 2121–2132. https://doi.org/10.1002/etc.5620121120.

Cipriano, L.A., Di Liberto, G., Tosoni, S., Pacchioni, G., 2020. Band gap in magnetic insulators from a charge transition level approach. J. Chem. Theory Comput. 16 (6), 3786–3798. https://doi.org/10.1021/acs.jctc.0c00134.

Coats, A.W., Redfern, J.P., 1964. Kinetic parameters from thermogravimetric data. Nature 201 (4914), 68–69. https://doi.org/10.1038/201068a0.

Delley, B., 2002. Hardness conserving semilocal pseudopotentials. Phys. Rev. B: Condens. Matter 66, (15). https://doi.org/10.1103/PhysRevB.66.155125 155125.

El-Asmy, A., Al-Ansi, T., Amin, R., Mounir, M., 1990. Spectral, magnetic and electrical properties of 1-succinyl bis (4-phenylthiosemicarbazide) complexes. Polyhedron 9 (17), 2029–2034. https://doi.org/10.1016/S0277-5387(00)84032-2.

El-Gammal, O.A., 2010. Synthesis, characterization, molecular modeling and antimicrobial activity of 2-(2-(ethylcarbamothioyl) hydrazinyl)-2-oxo-N-phenylacetamide copper complexes. Spectrochim. Acta, A 75 (2), 533–542. https://doi.org/10.1016/j.saa.2009.11.007.

El-Gazzar, A.B.A., Youssef, A.M.S., Youssef, M.M., Abu-Hashem, A.A., Badria, F.A., 2009. Design and synthesis of azolopyrimidoquinolines, pyrimidoquinazolines as anti-oxidant, anti-inflammatory and analgesic activities. Eur. J. Med. Chem. 44, 609–624. https://doi.org/10.1016/j.ejmech.2008.03.022.

El-Metwaly, N., Farghaly, T.A., Elghalban, M.G., 2020. Synthesis, analytical and spectral characterization for new VO (II)-triazole complexes; conformational study beside MOE docking simulation features. Appl. Organomet. Chem. 34, (4). https://doi.org/10.1002/aoc.5505 e5505.

El-Morshedy, R.M., El-Gamil, M.M., Abou-Elzahab, M.M., Abu El-Reash, G.M., 2019. Spectroscopic investigation, DFT, fluorescence, molecular docking and biological studies of divalent and trivalent binuclear complexes prepared from benzoyl thiosemicarbazide derivative of 2-benzylmalonohydrazide. Appl. Organomet. Chem. 33, (5). https://doi.org/10.1002/aoc.4871 e4871.

El-Sawaf, A.K., Abdel-Monem, Y.K., Azzam, M.A., 2020. Synthesis, spectroscopic, electrochemical characterization, density functional theory (DFT), time dependent density functional theory (TD-DFT), and antibacterial studies of some Co(II), Ni(II), and Cu(II) chelates of (E)-4-(1,5-dimethyl-3-oxo-2-phenyl-2,3-dihydro-1H-pyrazol-4-yl)-1-(3-hydroxynaphthalen-2-yl)methylene) thiosemicarbazide Schiff base ligand. Appl. Organomet. Chem. 34, (8). https://doi.org/10.1002/aoc.5729 e5729.

El-Sayed, M.-A.-A., El-Husseiny, W.M., Abdel-Aziz, N.I., El-Azab, A.S., Abuelizz, H.A., Abdel-Aziz, A.-A.-M., 2018. Synthesis and biological evaluation of 2-styrylquinolines as antitumour agents and EGFR kinase inhibitors: molecular docking study. J. Enzyme Inhib. Med. Chem. 33 (1), 199–209.

El-Sherif, A.A., Eldebss, T.M., 2011. Synthesis, spectral characterization, solution equilibria, in vitro antibacterial and cytotoxic activities of Cu(II), Ni(II), Mn(II), Co(II) and Zn(II) complexes with Schiff base derived from 5-bromosalicylaldehyde and 2-aminomethylthiophene. Spectrochim. Acta, A 79 (5), 1803–1814. https://doi.org/10.1016/j.saa.2011.05.062.

El-Sherif, A.A., Shoukry, M.M., Abd-Elgawad, M.M., 2012. Synthesis, characterization, biological activity and equilibrium studies of metal(II) ion complexes with tridentate hydrazone ligand derived from hydralazine. Spectrochim. Acta, A 98, 307–321. https://doi.org/10.1016/j.saa.2012.08.034.

Emam, S.M., Tolan, D.A., El-Nahas, A.M., 2020. Synthesis, structural, spectroscopic, and thermal studies of some transition-metal complexes of a ligand containing the amino mercapto triazole moiety. Appl. Organomet. Chem. 34, (5) https://onlinelibrary.wiley.com/doi/abs/10.1002/aoc.5591 e5591.

Fakhar, I., Yamin, B.M., Hasbullah, S.A., 2016. Synthesis and characterization of bis-thiourea having amino acid derivatives. AIP Conf. Proc., AIP Publishing LLC 030012.

Ferraro, J., Walker, W., 1965. Infrared spectra of hydroxy-bridged copper (II) compounds. Inorg. Chem. 4 (10), 1382–1386. https://doi.org/10.1021/ic50032a002.

Fukui, K., Yonezawa, T., Nagata, C., Shingu, H., 1954. Molecular orbital theory of orientation in aromatic, heteroaromatic, and other conjugated molecules. J. Chem. Phys. 22 (8), 1433–1442.

Gaber, M., Fayed, T.A., El-Gamil, M.M., El-Reash, G.M.A., 2018. Structural, thermogravimetric, B3LYP and biological studies on some heterocyclic thiosemicarbazide copper (II) complexes and evaluation of their molecular docking. J. Mol. Struct. 1151, 56–72. https://doi.org/10.1016/j.molstruc.2017.09.035.

Gaber, M., El-Ghamry, H.A., Fathalla, S.K., 2020. Synthesis, structural identification, DNA interaction and biological studies of divalent Mn, Co and Ni chelates of 3-amino-5-mercapto-1,2,4-triazole azo ligand. Appl. Organomet. Chem. 34, (4) https://onlinelibrary.wiley.com/doi/abs/10.1002/aoc.5678 e5678.

Govindarajan, M., Periandy, S., Carthigayen, K., 2012. FT-IR and FT-Raman spectra, thermo dynamical behavior, HOMO and LUMO, UV, NLO properties, computed frequency estimation analysis and electronic structure calculations on α-bromotoluene. Spectrochim. Acta, A 97, 411–422. https://doi.org/10.1016/j.saa.2012.06.028.

Hambley, T.W., 2009. Is anticancer drug development heading in the right direction? Cancer Res. 69 (4), 1259–1262.

Hammer, B., Hansen, L.B., Nørskov, J.K., 1999. Improved adsorption energetics within density-functional theory using revised Perdew-Burke-Ernzerhof functionals. Phys. Rev. B: Condens. Matter 59 (11), 7413. https://doi.org/10.1103/PhysRevB.59.7413.

Han, M.H., Yun, Y.-S., 2007. Mechanistic understanding and performance enhancement of biosorption of reactive dyestuffs by the waste biomass generated from amino acid fermentation process. Biochem. Eng. J. 36 (1), 2–7. https://doi.org/10.1016/j.bej.2006.06.010.

Hassani, R., Jabli, M., Kacem, Y., Marrot, J., Prim, D., Ben Hassine, B., 2015. New palladium-oxazoline complexes: synthesis and evaluation of the optical properties and the catalytic power during the oxidation of textile dyes. Beilstein J Org Chem 11, 1175–1186. https://doi.org/10.3762/bjoc.11.132.

R. Hernández-Molina, M.N. Sokolov, M. Clausen, W. Clegg, Synthesis and structure of nickel-containing cuboidal clusters derived from [W3Se4 (H2O) 9] 4 + . Site-differentiated substitution at the nickel site in the series [W3NiQ4 (H2O) 10] 4 + (Q = S, Se), Inorg. Chem. 45(26) (2006) 10567-10575. https://doi.org/10.1021/ic061146n.

Horowitz, H.H., Metzger, G., 1963. A new analysis of thermogravimetric traces. Anal. Chem. 35 (10), 1464–1468. https://doi.org/10.1021/ac60203a013.

Hosny, N.M., Mahmoud, H.M., Abdel-Rhman, M.H., 2018. Spectral, optical, and cytotoxicity studies on N-(2-isonicotinoylhydrazine-carbonothioyl)benzamide and its metal complexes. Heteroatom Chem. 29, (2). https://doi.org/10.1002/hc.21415 e21415.

Hosny, N.M., Hassan, N.Y., Mahmoud, H.M., Abdel-Rhman, M.H., 2018. Spectral, optical and cytotoxicity studies on 2-isonicotinoyl-N-phenylhydrazine-1-carboxamide(H3L) and some of its metal complexes. J. Mol. Struct. 1156, 602–611. https://doi.org/10.1016/j.molstruc.2017.11.114.

Hosny, N.M., Hussien, M.A., Motawa, R., Belal, A., Abdel-Rhman, M.H., 2020. Synthesis, spectral, modeling, docking and cytotoxicity studies on 2-(2-aminobenzoyl)-N-ethylhydrazine-1-carbothioamide and its divalent metal complexes. Appl. Organomet. Chem. 34 (11). https://doi.org/10.1002/aoc.5922.

Hosny, N.M., Belal, A., Motawea, R., Hussien, M.A., Abdel-Rhman, M.H., 2021. Spectral characterization, DFT, docking and cytotoxicity of N-benzyl-4,5-dihydro-3-methyl-5-oxo-1H-pyrazole-4-carbothioamide and its metal complexes. J. Mol. Struct. 1232,. https://doi.org/10.1016/j.molstruc.2021.130020 130020.

Integrated Computer-Aided Molecular Design Platform, Molecular operating environment, Chemical Computing Group, 2019.

Jeffery, G.H., Bassett, J., Mendham, J., Denney, R.C., 1989. Vogel'sTextbook of quantitative chemical analysis. John Wiley & Sons Inc, New York.

Jeragh, B., Al-Wahaib, D., El-Sherif, A.A., El-Dissouky, A., 2007. Potentiometric and thermodynamic studies of dissociation and metal complexation of 4-(3-Hydroxypyridin-2-ylimino)-4-phenylbutan-2-one. J. Chem. Eng. Data 52 (5), 1609–1614. https://doi.org/10.1021/je600586e.

Kenawy, I., Hafez, M., Lashein, R., 2001. Thermal decomposition of chloromethylated poly (styrene)-PAN resin and its complexes with some transition metal ions. J. Therm. Anal. Calorim. 65 (3), 723–736. https://doi.org/10.1023/a:1011999325998.

A. Kessi, B. Delley, Density functional crystal vs. cluster models as applied to zeolites, Int. J. Quantum Chem. 68(2) (1998) 135-144. https://doi.org/10.1002/(SICI)1097-461X(1998)68:2 < 135::AID-QUA6 > 3.0.CO;2-W.

Koch, A.L., 2003. Bacterial wall as target for attack: past, present, and future research. Clin. Microbiol. Rev. 16, 673–687. https://doi.org/10.1128/cmr.16.4.673-687.2003.

Lissi, E., Modak, B., Torres, R., Escobar, J., Urza, A., 1999. Total antioxidant potential of resinous exudates from Heliotropium species, and a comparison of the ABTS and DPPH methods. Free Rad. Res. 30, 471–477. https://doi.org/10.1080/10715769900300511.

Liu, L., Alam, M.S., Lee, D.-U., 2012. Synthesis, antioxidant activity and fluorescence properties of novel europium complexes with (E)-2-or 4-hydroxy-N'-[(2-hydroxynaphthalen-1-yl) methylene] benzohydrazide Schiff base. Bull. Korean Chem. Soc. 33 (10), 3361–3367. https://doi.org/10.5012/bkcs.2012.33.10.3361.

Maalik, A., Rahim, H., Saleem, M., Fatima, N., Rauf, A., Wadood, A., Malik, M.I., Ahmed, A., Rafique, H., Zafar, M.N., 2019. Synthesis, antimicrobial, antioxidant, cytotoxic, antiurease and molecular docking studies of N-(3-trifluoromethyl) benzoyl-N′-aryl thiourea derivatives. Bioorg. Chem. 88,. https://doi.org/10.1016/j.bioorg.2019.102946 102946.

Mahendiran, D., Pravin, N., Bhuvanesh, N.S.P., Kumar, R.S., Viswanathan, V., Velmurugan, D., Rahiman, A.K., 2018. Bis (thiosemicarbazone)copper(I) complexes as prospective therapeutic agents: interaction with DNA/BSA molecules, and in vitro and in vivo anti-proliferative activities. ChemistrySelect 3 (25), 7100–7111. https://doi.org/10.1002/slct.201800934.

Matesanz, A.I., Herrero, J.M., Faraco, E.J., Cubo, L., Quiroga, A.G., 2020. New platinum(II) triazole thiosemicarbazone complexes: analysis of their reactivity and potential antitumoral action. ChemBioChem. 21 (8), 1226–1232 https://chemistry-europe.onlinelibrary.wiley.com/doi/abs/10.1002/cbic.201900545.

Mauceri, H.J., Hanna, N.N., Beckett, M.A., Gorski, D.H., Staba, M.-J., Stellato, K.A., Bigelow, K., Heimann, R., Gately, S., Dhanabal, M., 1998. Combined effects of angiostatin and ionizing radiation in antitumour therapy. Nature 394 (6690), 287–291. https://doi.org/10.1038/28412.

Modeling and Simulation Solutions for Chemicals and Materials Research, Materials Studio, Accelrys software Inc., San Diego, USA, 2011.

Moore, J.W., Pearson, R.G., 1961. Kinetics and mechanism. John Wiley & Sons, New York.

Padmanabhan, J., Parthasarathi, R., Subramanian, V., Chattaraj, P., 2007. Electrophilicity-based charge transfer descriptor. J. Phys. Chem. A 111 (7), 1358–1361. https://doi.org/10.1021/jp0649549.

Pandey, R., Kumari, R., Sinha, S., Sahay, A., 1993. Thioamide bands and nature of bonding in the metal complexes of 3-(4-Pyridyl)-4-phenyl triazoline-5-thione. Asian J. Chem. 5 (3), 552.

Pandey, S.K., Singh, D.P., Marverti, G., Butcher, R.J., Pratap, S., 2018. Monodentate coordination of N, N′-disubstituted thiocarbamide ligands: syntheses, structural analyses, in vitro cytotoxicity and DNA damage studies of Cu(I) complexes. ChemistrySelect 3 (13), 3675–3679. https://doi.org/10.1002/slct.201800145.

Pandey, S.K., Pratap, S., Pokharia, S., Mishra, H., Marverti, G., Kaur, M., Jasinski, J.P., 2019. Copper (I) complexes based on novel N, N′-disubstituted thiocarbamides: Synthesis, spectroscopic, in vitro cytotoxicity, DNA damage and G0/G1 cell cycle arrest studies. Inorg. Chim. Acta 491, 105–117. https://doi.org/10.1016/j.ica.2019.04.007.

Parmar, N., Teraiya, S., Patel, R., 2010. Studies on oxovanadium (IV), Cr (III), Co (II), Ni (II), and Cu (II) chelates of some bisketimino ligands. J. Coord. Chem. 63 (18), 3279–3290. https://doi.org/10.1080/00958972.2010.508516.

Pearson, R.G., 1989. Absolute electronegativity and hardness: applications to organic chemistry. J. Org. Chem. 54 (6), 1423–1430. https://doi.org/10.1021/jo00267a034.

Pfaller, M.A., Burmeister, L., Bartlett, M.S., Rinaldi, M.G., 1988. Multicenter evaluation of four methods of yeast inoculum preparation. J. Clin. Microbiol. 26 (8), 1437–1441.

Rahman, F.U., Bibi, M., Altaf, A.A., Tahir, M.N., Ullah, F., Khan, E., 2020. Zn, Cd and Hg complexes with unsymmetric thiourea derivatives; syntheses, free radical scavenging and enzyme inhibition essay. J. Mol. Struct. 1211,. https://doi.org/10.1016/j.molstruc.2020.128096 128096.

Rakha, T.H., 2000. Transition metal chelates derived from potassium nicotinoyldithiocarbazate (KHNDC). Synth. React. Inorg. Met.-Org. Chem. 30 (2), 205–224. https://doi.org/10.1080/00945710009351758.

Rakha, T.H., Ibrahim, K.M., Khalifa, M.I., 1989. Thermochemical study of some transition metal complexes of isonicotinic hydrazide derivatives. Thermochim. Acta 144 (1), 53–63. https://doi.org/10.1016/0040-6031(89)85084-1.

Rastogi, D., Sharma, K., 1974. Stereochemical features of some nickel (II) and cobalt (II) complexes of amino ligand—2-(2-aminoethyl) pyridine-VII. J. Inorg. Nucl. Chem. 36 (10), 2219–2228. https://doi.org/10.1016/0022-1902(74)80258-7.

Razak, N.H.A., Tan, L.L., Hasbullah, S.A., Heng, L.Y., 2020. Reflectance chemosensor based on bis-thiourea derivative as ionophore for copper (II) ion detection. Microchem. J. 153,. https://doi.org/10.1016/j.microc.2019.104460 104460.

Robinson, T., Chandran, B., Nigam, P., 2002. Removal of dyes from a synthetic textile dye effluent by biosorption on apple pomace and wheat straw. Water Res. 36 (11), 2824–2830. https://doi.org/10.1016/S0043-1354(01)00521-8.

Etaiw, S.E.d.H., Fayed, T.A., El-bendary, M.M., Marie, H., 2018. Three-dimensional coordination polymers based on trimethyltin cation with nicotinic and isonicotinic acids as anticancer agents. Appl. Organomet. Chem. 32, (2). https://doi.org/10.1002/aoc.4066 e4066.

Saha, S., Jana, S., Gupta, S., Ghosh, A., Nayek, H.P., 2016. Syntheses, structures and biological activities of square planar Ni(II), Cu(II) complexes. Polyhedron 107, 183–189. https://doi.org/10.1016/j.poly.2016.01.034.

Santos, V.P., Pereira, M.F., Faria, P.C., Orfao, J.J., 2009. Decolourisation of dye solutions by oxidation with H(2)O(2) in the presence of modified activated carbons. J. Hazard. Mater. 162 (2–3), 736–742. https://doi.org/10.1016/j.jhazmat.2008.05.090.

Shah, R., Alharbi, A., Hameed, A.M., Saad, F., Zaky, R., Khedr, A. M., El-Metwaly, N., 2020. Synthesis and structural elucidation for new schiff base complexes, conductance, conformational, MOE-docking and biological studies. J. Inorg. Organomet. Polym. Mater. 30 (9), 3595–3607. https://doi.org/10.1007/s10904-020-01505-w.

Singh, H.L., Varshney, S., Varshney, A.K., 1999. Organotin (IV) complexes of biologically active Schiff bases derived from heterocyclic ketones and sulpha drugs. Appl. Organomet. Chem. 13 (9), 637–641. https://doi.org/10.1002/(SICI)1099-0739(199909)13:9<637::AID-AOC919>3.0.CO;2-K.

Sogabe, S., Kawakita, Y., Igaki, S., Iwata, H., Miki, H., Cary, D.R., Takagi, T., Takagi, S., Ohta, Y., Ishikawa, T., 2013. Structure-based approach for the discovery of pyrrolo [3, 2-d] pyrimidine-based EGFR T790M/L858R mutant inhibitors. ACS Med. Chem. Lett. 4 (2), 201–205. https://doi.org/10.1021/ml300327z.

Tanak, H., Koysal, Y., Isik, S., Yaman, H., Ahsen, V., 2011. Experimental and computational approaches to the molecular structure of 3-(2-Mercaptopyridine) phthalonitrile. Bull. Korean Chem. Soc. 32 (2), 673–680. https://doi.org/10.5012/bkcs.2011.32.2.673.

Thompson, K.H., Orvig, C., 2003. Boon and bane of metal ions in medicine. Science 300 (5621), 936–939.

I. Tossidis, C. Bolos, P. Aslanidis, G. Katsoulos, Monohalogenobenzoylhydrazones III. Synthesis and structural studies of Pt(II), Pd (II) and Rh(III) complexes of Di-(2-pyridyl) ketonechlorobenzoyl hydrazones, Inorg. Chim. Acta 133(2) (1987) 275-280. https://doi.org/10.1016/S0020-1693(00)87779-8.

L.G.V. Uitert, C.G. Haas, Studies on coördination compounds. I. A method for determining thermodynamic equilibrium constants in mixed solvents1, 2, J. Am. Chem. Soc. 75(2) (1953) 451-455. https://doi.org/10.1021/ja01098a057.

Velumani, S., Mathew, X., Sebastian, P., Narayandass, S.K., Mangalaraj, D., 2003. Structural and optical properties of hot wall deposited CdSe thin films. Sol. Energy Mater. Sol. Cells 76 (3), 347–358.

J.H. Warren, Ab initio molecular orbital theory, Wiley-Interscience1986.

Yahyazadeh, A., Ghasemi, Z., 2013. Synthesis of unsymmetrical thiourea derivatives. Eur. Chem. Bull. 2 (8), 573–575. https://doi.org/10.17628/ecb.2013.2.573-575.

Yousef, T.A., El-Reash, G.M.A., El Morshedy, R.M., 2012. Quantum chemical calculations, experimental investigations and DNA studies on (E)-2-((3-hydroxynaphthalen-2-yl) methylene)-N-(pyridin-2-yl) hydrazinecarbothioamide and its Mn (II), Ni (II), Cu (II), Zn (II) and Cd (II) complexes. Polyhedron 45 (1), 71–85. https://doi.org/10.1016/j.poly.2012.07.041.

Yousef, T.A., El-Reash, G.M.A., El-Gammal, O.A., Ahmed, S.F., 2014. Structural, DFT and biological studies on Cu (II) complexes of semi and thiosemicarbazide ligands derived from diketo hydrazide. Polyhedron 81, 749–763. https://doi.org/10.1016/j.poly.2014.07.035.

Zaky, R.R., Yousef, T.A., Abdelghany, A.M., 2014. Computational studies of the first order kinetic reactions for mononuclear copper (II) complexes having a hard–soft NS donor ligand. Spectrochim. Acta, A 130, 178–187. https://doi.org/10.1016/j.saa.2014.02.173.

Zalaoglu, Y., Ulgen, A., Terzioglu, C., Yildirim, G., 2010. Theoretical study on the characterization of 6-methyl 1, 2, 3, 4-tetrahydroquinoline using quantum mechanical calculation methods. Fen Bilimleri Dergisi 14, 66–76.

Zhao, P.S., Wang, H.Y., Song, J., Lu, L.D., 2010. Synthesis, structures, and property studies on Zn(II), Ni(II), and Cu(II) complexes with a Schiff base ligand containing thiocarbamide group. Struct. Chem. 21 (5), 977–987. https://doi.org/10.1007/s11224-010-9634-6.